

Delay-Aware Hierarchical Federated Learning

Frank Po-Chen Lin, *Student Member, IEEE*,

Seyyedali Hosseinalipour, *Member, IEEE*, Nicolò Michelusi, *Senior Member, IEEE*,

and Christopher G. Brinton, *Senior Member, IEEE*

Abstract

Federated learning has gained popularity as a means of training models distributed across the wireless edge. The paper introduces delay-aware hierarchical federated learning (DFL) to improve the efficiency of distributed machine learning (ML) model training by accounting for communication delays between edge and cloud. Different from traditional federated learning, DFL leverages multiple stochastic gradient descent iterations on local datasets within each global aggregation period and intermittently aggregates model parameters through edge servers in local subnetworks. During global synchronization, the cloud server consolidates local models with the outdated global model using a local-global combiner, thus preserving crucial elements of both, enhancing learning efficiency under the presence of delay. A set of conditions is obtained to achieve the sub-linear convergence rate of $\mathcal{O}(1/k)$ for strongly convex and smooth loss functions. Based on these findings, an adaptive control algorithm is developed for DFL, implementing policies to mitigate energy consumption and communication latency while aiming for sublinear convergence. Numerical evaluations show DFL's superior performance in terms of faster global model convergence, reduced resource consumption, and robustness against communication delays compared to existing FL algorithms. In summary, this proposed method offers improved efficiency and results when dealing with both convex and non-convex loss functions.

Index Terms

Federated learning, edge intelligence, network optimization, convergence analysis, hierarchical architecture.

F. Lin and C. Brinton are with the School of Electrical and Computer Engineering, Purdue University, IN, USA. e-mail: {lin1183,cgb}@purdue.edu. Brinton and Lin acknowledge support from ONR grants N000142212305 and N000142112472.

S. Hosseinalipour is with the Department of Electrical Engineering, University at Buffalo, NY, USA. e-mail: alipour@buffalo.edu.

N. Michelusi is with the School of Electrical, Computer and Energy Engineering, Arizona State University, AZ, USA. e-mail: nicolo.michelusi@asu.edu. Part of his research has been funded by NSF under grant CNS-2129015.

A condensed version of this paper was presented at IEEE Globecom 2020 [1].

Machine Learning (ML) has become a popular tool for carrying out a variety of practical applications in computer vision, speech recognition, natural language processing, and robotic control [2]–[4]. Conventionally, ML model training for these applications is conducted in a centralized manner, where data from different sources is collected and processed in a single server/datacenter. Nevertheless, in many applications, data used for model training is generated/gathered at the modern Internet-of-Things (IoT) devices located at the edge of the network (e.g., autonomous vehicles, mobile phones, and wearable devices) [5], which makes centralized model training impractical. In fact, transferring the massive amount of data collected from the IoT devices to a central location imposes high latency and power/resource consumption [6], which is not desired especially in real-time applications [2], [7]. Also, privacy concerns related to transmitting private data across the network have progressively advocated for storing data locally and shifting the ML model training to the network edge where the data gets collected. This has led to an emerging area of distributed ML over the network edge, which exploits the distributed computing power of IoT devices to realize an intelligent edge/fog [8], [9].

Federated learning (FL) [10], a popular distributed ML framework, trains an ML model via engaging edge devices in collaborative model training while keeping their data locally. It does so by executing three steps repeatedly: (i) *local model training* at each edge device using its local dataset, (ii) *aggregation of the local models* to a global model by a server, and (iii) *synchronization of the local models* with the newly obtained global model. Upon being implemented over a real-world network edge, FL faces many challenges and design problems given the heterogeneities existing at the wireless edge [8], [11]. (i) *Extreme Data Heterogeneity*: the local datasets of the devices may exhibit significant heterogeneity, making them non-independent and identically distributed (non-i.i.d.), causing the locally trained models in each edge device to be significantly biased towards the local dataset [8]. (ii) *Delay of Model Aggregations*: Variable distances and quality of communications between the edge devices and the point of aggregation (e.g., a cloud server) may result in considerable model aggregation and synchronization delays, making naive synchronization of the received global model with the local model impractical [1]. (iii) *Hierarchical Architecture of Network Edge*: Large-scale edge networks do not admit the conventional FL network architecture. In particular, edge devices are often not directly connected to a cloud server, instead, they are connected to the edge servers, which facilitate the communication to the cloud server [12]. In this paper, we are motivated to address the above three challenges. In particular, we consider model training under a metric of data heterogeneity extended from the current art,

which can capture extreme cases of data diversity across the devices. Also, we explicitly account for the delay in model aggregation and introduce a linear local-global model combining scheme. This scheme retains essential elements of both the outdated global model and the current local model, thereby improving the overall learning efficiency. Our methodology can augment existing studies by incorporating our strategy with those already established. Finally, we consider model training over a realistic hierarchical network edge architecture.

Summary of Contributions:

Our contributions in this work can be summarized as follows:

- We propose *delay-aware federated learning* (DFL), a novel methodology for improving distributed ML model training efficiency by accounting for the round-trip delay between edge and cloud. DFL accounts for the effects of delays by introducing a local-global model combiner scheme during global synchronization, which conserve vital aspects of both the stale global model and the current local model, thereby enhancing overall learning efficiency.
- We theoretically investigate the convergence behavior of DFL under a generalized data heterogeneity metric. Our convergence analysis introduces new techniques, such as coupled dynamic systems, to the current art in hierarchical FL [12]–[17]. We obtain a set of conditions to achieve the sub-linear convergence rate of $\mathcal{O}(1/k)$ for strongly convex and smooth loss functions while mitigating the communication delay, which resembles the convergence rate of stochastic gradient descent in centralized model training without delay.
- Leveraging the convergence characteristics, we introduce an adaptive control algorithm for DFL, which targets a joint optimization of communication energy, latency, and ML performance while preserving a sub-linear convergence rate. This involves solving a non-convex integer programming problem, adapting (i) the global aggregation interval with the cloud, (ii) the local aggregation interval with the edge servers, (iii) the learning rate, and (iv) the combiner weight over time.
- Our numerical evaluations demonstrate the effectiveness of DFL in terms of convergence speed and resource consumption under various network settings, under both convex and non-convex loss functions. We observe that DFL achieves (i) faster convergence of the global model, (ii) reduced resource consumption, and (iii) improved robustness against communication delays compared to existing FL algorithms.

The structure of this paper is as follows: Section I delves into works related to this study,

specifically addressing the challenges mentioned in Federated Learning (FL). Subsequently, Section II outlines the system model and details the machine learning methodology implemented in DFL. A theoretical analysis of DFL's convergence behavior is provided in Section III, followed by a discussion on our adaptive control algorithm designed to optimize controllable parameters within DFL in Section IV. Lastly, Section V showcases numerical experiments conducted to assess the performance of DFL. For brevity, proofs are provided as sketches with full versions in the appendices.

I. RELATED WORK

We categorize the related work to this study with respect to the three aforementioned challenges of FL. For a comprehensive survey of works on FL, we refer the interested reader to [18].

Non-i.i.d. Data Across the Devices. Non-i.i.d data across the devices has been shown to significantly reduce the performance of FL due to local model bias [10]. To counteract this effect, [19], [20] tunes the frequency of global model aggregations, [21], [22] conduct data transfer across the devices to reduce the heterogeneity of data, and [23]–[25] conduct efficient resource allocation under non-i.i.d. data. However, most of these works rely on a simple modeling of non-i.i.d. data across the devices which cannot be generalized to real-world settings. Recently, we introduced a new metric of data heterogeneity in [26] that extends the current art and is able to capture extreme non-i.i.d. data across the devices. However, in [26], this metric is exploited in a completely different framework, where devices conduct local device-to-device (D2D) communications for model consensus, as compared to this works. In this work, we aim to conduct convergence analysis of model training under this general data heterogeneity metric, while taking into account for communication delay and hierarchical network architecture.

Model Training under Delay Considerations. Upstream/downstream communication between the edge and server can often lead to non-negligible transmission delays in FL. Delay of model training in FL has been modeled and considered in several recent works [23], [27]–[31]. These works model the delay with respect to the channel conditions between the devices and the server and the devices' local computation power. The delay is often aimed to be minimized in these works to have the fastest model training scheme. However, none of these works aim to *mitigate* the impact of delay via intelligent synchronization of the received global model and the local model at the devices. In this work, we study this under-explored topic via proposing a linear local-global model combiner.

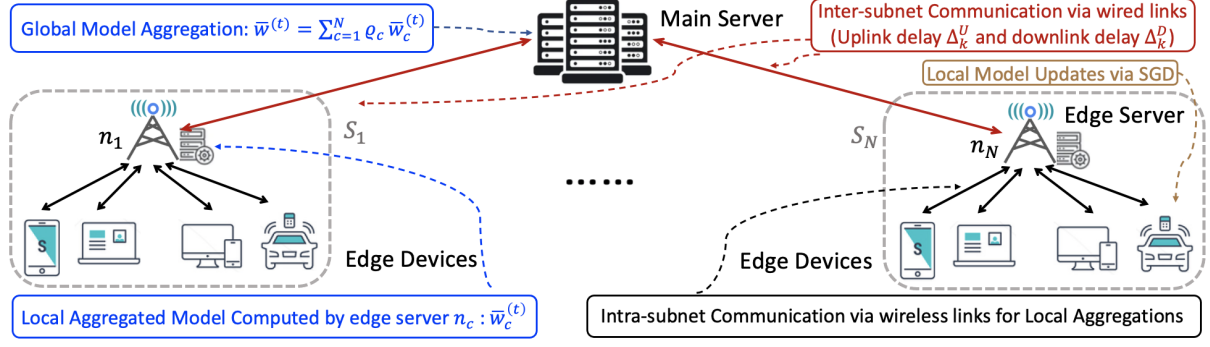


FIGURE 1: The three-layer hierarchical federated learning network architecture consists of edge devices forming local subnet topologies based on their proximity to the local aggregator.

Hierarchical Federated Learning. Several studies have aimed to propose new system architectures to improve the scalability of ML model training in FL [12], [26], [32]–[34]. Specifically, hierarchical federated learning has been proposed as a realistic system model, which allows edge devices to first transmit their local model parameters to edge servers for intermediate aggregation before edge servers conduct global aggregation through a cloud server, which reduces the frequency of performing resource intensive global aggregations [12]–[17]. This architecture has been investigated through the lens of resource allocation [13], [15], and edge association [12], [14], [16], [17]. Although these works provide valuable design insights, they mostly consider a simplistic data heterogeneity metric and do not take into account for smart local synchronization of the local models with the global model. As compared to these works, we introduce a new ML convergence analysis scheme that takes into account for a generalized data heterogeneity metric under a new linear local-global model combiner scheme. Drawing from the convergence properties, we devise a control algorithm for DFL, which incorporates strategies aimed at mitigating energy consumption and communication latency.

II. SYSTEM MODEL AND MACHINE LEARNING METHODOLOGY

In this section, we first describe our hierarchical edge network system model (Sec. II-A) and formalize the ML task under consideration (Sec. II-B). Then, we develop our delay-aware federated learning procedure, DFL (Sec. II-C). A list of acronyms and symbols used is provided in Table I and II.

A. Edge Network System Model

We consider ML model learning over the hierarchical network architecture depicted in Fig. 1. The network consists of three layers of nodes. At the top of the hierarchy, a main server (e.g., a cloud server) is in charge of global model aggregations. In the middle of the hierarchy, there are N edge servers (e.g., coexisting with cellular base stations), collected via the set $\mathcal{N} = \{n_1, \dots, n_N\}$, which act as local model aggregators. Finally, at the bottom of the hierarchy, there are I edge devices represented via the set $\mathcal{I} = \{1, \dots, I\}$ in charge of local model training. The edge devices are organized into subnets (subnetworks), with a one-to-one mapping between the subnets and the edge servers, providing them uplink/downlink connectivity. In particular, the devices are partitioned into N sets $\{\mathcal{S}_c\}_{c=1}^N$, where set \mathcal{S}_c is associated with edge server $n_c \in \mathcal{N}$ for uplink/downlink model transmissions, with $\mathcal{S}_c \cap \mathcal{S}_{c'} = \emptyset \ \forall c \neq c'$ and $\cup_{c=1}^N \mathcal{S}_c = \mathcal{I}$. Each subnet \mathcal{S}_c consists of $s_c = |\mathcal{S}_c|$ edge devices, where $\sum_{c=1}^N s_c = I$.¹

TABLE I: List of acronyms

Acronym	Definition	Acronym	Definition
ML	Machine Learning	FL	Federated Learning
DFL	Delay-Aware Federated Learning	SGD	Stochastic Gradient Descent
SVM	Support Vector Machine	CNN	Convolutional Neural Network

B. Machine Learning Model

We assume that each edge device $i \in \mathcal{I}$ owns a dataset \mathcal{D}_i with $D_i = |\mathcal{D}_i|$ data points. In general, the \mathcal{D}_i 's are non-i.i.d. (non-independent and identically distributed), i.e., there exists statistical dataset diversity across the devices. Each data point $(\mathbf{x}, y) \in \mathcal{D}_i, \forall i$, consists of an m -dimensional feature vector $\mathbf{x} \in \mathbb{R}^m$ and a label $y \in \mathbb{R}$. We let $\ell(\mathbf{x}, y; \mathbf{w})$ denote the *loss* associated with data point (\mathbf{x}, y) under *ML model parameter vector* $\mathbf{w} \in \mathbb{R}^M$, where M denotes the dimension of the model. The loss quantifies the precision of the ML model with respect to the underlying ML task; for example, in linear regression, $\ell(\mathbf{x}, y; \mathbf{w}) = \frac{1}{2}(y - \mathbf{w}^\top \mathbf{x})^2$. The *local loss function* at device i is defined as

$$F_i(\mathbf{w}) = \frac{1}{D_i} \sum_{(\mathbf{x}, y) \in \mathcal{D}_i} \ell(\mathbf{x}, y; \mathbf{w}). \quad (1)$$

¹This model is capable of being adapted to time-varying topologies, for instance, mobile devices switching subnet. However, we omit this for notational simplicity.

TABLE II: List of key symbols

Symbol	Description	Symbol	Description
\mathcal{N}	Set of all edge servers	N	Number of all edge servers
\mathcal{I}	Set of all edge devices	I	Number of all edge devices
\mathcal{S}_c	Set of edge devices in subnet c	s_c	Number of edge devices in subnet c
n_c	Index of local model aggregator (edge server)	$\ell(\cdot)$	Loss function associated with each datapoint
\mathcal{D}_i	Dataset of edge devices i	D_i	Number of data points in edge device i
$F_i(\cdot)$	Local loss function for device i	$\bar{F}_c(\cdot)$	Subnet loss function for subnet c
$F(\cdot)$	Global loss function	\mathbf{w}^*	Optimal global model
δ, ζ	Inter-gradient diversity parameters across subnets	δ_c, ζ_c	Intra-gradient diversity parameters in subnet c
t	Time index of local model training iteration	k	Index of local model training interval
\mathcal{T}_k	k -th local model training interval	τ_k	Length of the k -th local model training interval
$\mathcal{T}_{k,c}^L$	Set of local aggregation instances in the k -th local model training interval	$\hat{\mathbf{g}}_i^{(t)}$	Local stochastic gradient at device i and time t
$\mathbf{w}_i^{(t)}$	Local model at device i and time t	$\tilde{\mathbf{w}}_i^{(t)}$	Tentative Local model at device i and time t
$\bar{\mathbf{w}}_c^{(t)}$	Instantaneous aggregated local model across devices $i \in \mathcal{S}_c$	$\bar{\mathbf{w}}^{(t)}$	Global model at time t
$\Theta_c^{(t)}$	Indicator of local aggregation for subnet c	α_k	Combiner weight for the linear local-global combiner
Δ_k^U	Upstream delay between edge device and main server	Δ_k^D	Downstream delay between edge device and main server

We subsequently define the *subnet loss function* for each \mathcal{S}_c as the average loss of devices in the subnet, i.e.,

$$\bar{F}_c(\mathbf{w}) = \sum_{i \in \mathcal{S}_c} \rho_{i,c} F_i(\mathbf{w}), \quad (2)$$

where $\rho_{i,c} = D_i / \sum_{j \in \mathcal{S}_c} D_j$ is the weight associated with edge device $i \in \mathcal{S}_c$ relative to its respective subnet. The *global loss function* is defined as the average loss across the subnets

$$F(\mathbf{w}) = \sum_{c=1}^N \varrho_c \bar{F}_c(\mathbf{w}), \quad (3)$$

where $\varrho_c = \sum_{i \in \mathcal{S}_c} D_i / \sum_{j \in \mathcal{I}} D_j$ is the weight associated with subnet \mathcal{S}_c relative to the network.

The goal of ML model training is to find the optimal global model parameter vector $\mathbf{w}^* \in \mathbb{R}^M$:

$$\mathbf{w}^* = \arg \min_{\mathbf{w} \in \mathbb{R}^M} F(\mathbf{w}). \quad (4)$$

In the following, we introduce some assumptions regarding the above-defined loss functions that are commonly employed in distributed ML literature [19], [24], [35], [36]. These assumptions further imply the existence and uniqueness of \mathbf{w}^* .

Assumption 1 (Loss Functions Characteristics). *Henceforth, the following assumptions are made:*

- **Strong convexity:** Each local loss function F_i is μ -strongly convex $\forall i \in \mathcal{I}$, i.e.,

$$F_i(\mathbf{w}_1) \geq F_i(\mathbf{w}_2) + \nabla F_i(\mathbf{w}_2)^\top (\mathbf{w}_1 - \mathbf{w}_2) + \frac{\mu}{2} \|\mathbf{w}_1 - \mathbf{w}_2\|^2, \forall \mathbf{w}_1, \mathbf{w}_2 \in \mathbb{R}^M. \quad (5)$$

where $\|\cdot\|$ refers to the Euclidean norm.

- **Smoothness:** Each local loss function F_i is β -smooth $\forall i \in \mathcal{I}$, i.e.,

$$\|\nabla F_i(\mathbf{w}_1) - \nabla F_i(\mathbf{w}_2)\| \leq \beta \|\mathbf{w}_1 - \mathbf{w}_2\|, \forall \mathbf{w}_1, \mathbf{w}_2 \in \mathbb{R}^M, \quad (6)$$

where $\beta > \mu$. These assumptions imply the strong convexity and β -smoothness of \bar{F}_c and F .²

The above assumptions are leveraged in our theoretical analysis in Sec. III, and subsequently to develop the control algorithm in Sec. IV. Our experiments in Sec. V demonstrate the effectiveness of our methodology, even for non-convex loss functions (e.g., neural networks).

We next introduce measures of gradient diversity to quantify the statistical heterogeneity across local datasets. Different from our existing work [26], we consider this both across and within subnets, which will be important to our analysis:

Definition 1 (Inter-Subnet Gradient Diversity). *The inter-subnet gradient diversity across the device subnets is measured via two non-negative constants δ, ζ that satisfy*

$$\|\nabla \bar{F}_c(\mathbf{w}) - \nabla F(\mathbf{w})\| \leq \delta + \zeta \|\mathbf{w} - \mathbf{w}^*\|, \forall c, \mathbf{w}. \quad (7)$$

Definition 2 (Intra-Subnet Gradient Diversity). *The intra-subnet gradient diversity across the devices belonging to subnet \mathcal{S}_c is measured via non-negative constants δ_c, ζ_c that satisfy*

$$\|\nabla F_i(\mathbf{w}) - \nabla \bar{F}_c(\mathbf{w})\| \leq \delta_c + \zeta_c \|\mathbf{w} - \mathbf{w}^*\|, \forall i \in \mathcal{S}_c, \forall c, \mathbf{w}. \quad (8)$$

The definitions of gradient diversity are used to measure the degree of heterogeneity across the local datasets of devices in federated learning settings, which may be non-i.i.d., and can impact the convergence performance. A high value of gradient diversity implies a large dissimilarity between the local datasets and the global data distributions. We further define ratios $\omega = \frac{\zeta}{2\beta} \leq 1$ and $\omega_c = \frac{\zeta_c}{2\beta} \leq 1$, which will be important in our analysis. The above definitions are obtained using the β -smoothness of the loss functions. Specifically, for (7),

$$\|\nabla \bar{F}_c(\mathbf{w}) - \nabla F(\mathbf{w})\| = \|\nabla \bar{F}_c(\mathbf{w}) - \nabla \bar{F}_c(\mathbf{w}^*) + \nabla \bar{F}_c(\mathbf{w}^*) + \underbrace{\nabla F(\mathbf{w}^*) - \nabla F(\mathbf{w})}_{=0}\|$$

²Throughout, $\|\cdot\|$ is used to denote 2-norm of the vectors.

$$\leq \|\nabla \bar{F}_c(\mathbf{w}) - \nabla \bar{F}_c(\mathbf{w}^*)\| + \|\nabla \bar{F}_c(\mathbf{w}^*)\| + \|\nabla F(\mathbf{w}) - \nabla F(\mathbf{w}^*)\| \leq \delta + 2\beta\|\mathbf{w} - \mathbf{w}^*\|, \quad (9)$$

where $\|\nabla \bar{F}_c(\mathbf{w}^*)\| \leq \delta$. The bound in (9) demonstrates the fact that by applying the smoothness property of the functions $\bar{F}_c(\cdot)$ and $F(\cdot)$ along with imposing an upper bounded δ on the subnet gradients at the optimum, the definition of gradient diversity in (8) is a general expression for (9), which in turn results in (7) for $\frac{\zeta}{2\beta} \leq 1$. Using the same steps (8) can be obtained, as we discuss in [26]. These gradient diversity metrics extend the conventional definition of gradient diversity used in literature, e.g., as in [19], which is a special case of (7) and (8) with $\zeta = \zeta_c = 0, \forall c$. Given that in FL settings, the local dataset of the devices may be extremely non-i.i.d., very large values of δ and δ_c in (7) and (8) are required when $\zeta = \zeta_c = 0$, which will, in turn, make the convergence bounds very loose and ineffective in describing the system behavior. The addition of terms with coefficients ζ, ζ_c in (7) and (8) will lead to bounded values for δ and δ_c , especially in the beginning of training when $\|\mathbf{w} - \mathbf{w}^*\|$ can take an arbitrary large value. At the same time, the addition of ζ, ζ_c in (7), (8) forms a coupling between the gradient diversity and the optimality gap $\|\mathbf{w} - \mathbf{w}^*\|$. As we will see, this coupling makes our convergence analysis unique from the current art and rather non-trivial.

C. DFL: Delay-Aware Federated Learning

1) Overview and Rationale: In the context of DFL, the process of training the ML model comprises of a sequence of local model training intervals that occur between two successive *global synchronizations*, which are subsequently followed from *global aggregations*. During each interval, the edge devices carry out stochastic gradient descent (SGD) iterations based on their local data to optimize their local loss functions $F_i(\cdot)$, $\forall i$. Additionally, the edge server conducts aperiodic *local aggregations*³ to synchronize the local model parameters with the edge devices within its corresponding subnet. Aggregation refers to computing an *aggregated model* by taking the weighted average of local models from edge devices. In contrast, synchronization refers to updating local models at edge devices using the aggregated model obtained after aggregation. On one hand, local aggregations are conducted within subnets through device-to-edge communication links, resulting in small-scale communication delays because edge servers are typically physically

³Note that in Fig. 2, the parameters m_1 and m_2 may not be equal. In fact, DFL allows for aperiodic local aggregations during each local model training interval, the frequency of which will be later tuned in our control algorithms to mitigate network resource consumption.

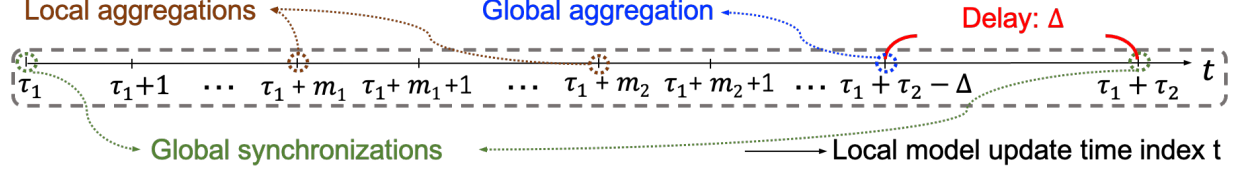


FIGURE 2: Illustration of the timescale in DFL. The time index t represents local model updates through SGD, local aggregation, as well as global aggregations and synchronizations.

closer to the edge devices. On the other hand, global aggregations occur across the entire network through edge-to-cloud communication links, which typically have non-negligible propagation delays in the range of hundreds of milliseconds to several seconds, depending on network bandwidth [37]. This delay can significantly degrade learning performance in FL because the main server is often far from the edge devices. In this paper, we neglect the delay of local aggregations within subnets and focus on the global aggregation delay, assuming device-to-edge links have a much shorter range than edge-to-cloud links. Details of the DFL procedure and the modeling of communication delay will be described in the following.

2) *DFL Model Training Procedure*: In the following, we provide a high-level description of our methodology, which will be later formalized in Sec. II-C3. We consider a slotted-time representation of a network where each edge device conducts a *local model training iteration* via SGD at each time index $t = 0, 1, \dots, T$. The time duration of 0 to T is partitioned into multiple *local model training intervals* indexed by $k = 0, 1, \dots, K - 1$, each capturing time interval $\mathcal{T}_k = \{t_k + 1, \dots, t_{k+1}\} \subset \{0, 1, \dots, T\}$. The model training procedure at the devices starts with the server broadcasting the initial global model $\bar{\mathbf{w}}^{(0)}$ to all the devices at $t_0 = 0$, proceeding through a series of global aggregations. Local model training intervals occur in between two consecutive global model synchronizations at time t_k and t_{k+1} , during which the local models of devices are updated via SGD. At each instance of global aggregation, the models of the devices are collected (i.e., they engage in uplink transmissions) and arrive at the server with a certain delay. The server will then aggregate the received models into a global model and broadcast it (i.e., engage in downlink transmission) to the devices, which involves another delay. In parallel, devices proceed with local updates before the global model arrives. Upon reception of the global model, devices synchronize their local models in a manner accounting for both uplink and downlink delays. The relationships between the timescales are depicted in Fig. 2.

The length of the k th local model training interval is denoted by $\tau_k = |\mathcal{T}_k|$. We have $t_k =$

$\sum_{\ell=0}^{k-1} \tau_\ell$, $\forall k$, where $t_0 = 0$ and $t_K = T$. This allows for varying the length of local model training intervals across global synchronizations (i.e., possibly $\tau_k \neq \tau_{k'}$ for $k \neq k'$). During the k th local model training interval, we define $\mathcal{T}_{k,c}^L \subset \mathcal{T}_k$ as the set of time instances when the edge server pulls the models of devices in subnet \mathcal{S}_c (i.e., devices engage in uplink transmissions) and performs local aggregations of their models. Local aggregation synchronizes the local models within the same subnet by computing their weighted average. We next formalize the above procedure.

3) *Formalizing DFL*: Next, we formalize the local training, local model aggregations, and global model aggregation and synchronization. Through this process, we will also introduce new notions used for orchestrating the formulation of the system.

Definition 3 (Conditional Expectation). $\mathbb{E}_t(\cdot)$ represents the conditional expectation conditioned on \mathcal{F}_t , where \mathcal{F}_t denotes the σ -algebra generated by all random sampling up to but excluding, t .

Local SGD iterations: At $t \in \mathcal{T}_k$, device i randomly samples a mini-batch $\xi_i^{(t)}$ of datapoints from its local dataset \mathcal{D}_i , and uses it to calculate the unbiased *stochastic gradient estimate* using its previous local model $\mathbf{w}_i^{(t)}$ as

$$\hat{\mathbf{g}}_i^{(t)} = \frac{1}{|\xi_i^{(t)}|} \sum_{(\mathbf{x}, y) \in \xi_i^{(t)}} \nabla \ell(\mathbf{x}, y; \mathbf{w}_i^{(t)}). \quad (10)$$

Tentative Local Model: Using the gradient estimate $\hat{\mathbf{g}}_i^{(t-1)}$, each device computes its *tentative local model* $\tilde{\mathbf{w}}_i^{(t)}$ as

$$\tilde{\mathbf{w}}_i^{(t)} = \mathbf{w}_i^{(t-1)} - \eta_k \hat{\mathbf{g}}_i^{(t-1)}, \quad t \in \mathcal{T}_k, \quad (11)$$

where $\eta_k > 0$ denotes the step size. We denote this tentative because it is an intermediate calculation prior to any potential aggregation. Specifically, based on $\tilde{\mathbf{w}}_i^{(t)}$, the *updated local model* $\mathbf{w}_i^{(t)}$ is computed either through setting it to $\tilde{\mathbf{w}}_i^{(t)}$ or through a local aggregation, discussed next.

Updated Local Model: At time t , if subnet \mathcal{S}_c does not conduct a local aggregation, i.e., $t \in \mathcal{T}_k \setminus \mathcal{T}_{k,c}^L$, the final updated local model is obtained based on the conventional rule $\mathbf{w}_i^{(t)} = \tilde{\mathbf{w}}_i^{(t)}$ from (11). Otherwise, i.e., if $t \in \mathcal{T}_{k,c}^L$, then each device i in subnet \mathcal{S}_c transmits its tentative updated local model $\tilde{\mathbf{w}}_i^{(t)}$ to edge server n_c which computes the *instantaneous aggregated local model* as follows:

$$\bar{\mathbf{w}}_c^{(t)} = \sum_{i \in \mathcal{S}_c} \rho_{i,c} \tilde{\mathbf{w}}_i^{(t)}. \quad (12)$$

The edge server n_c then broadcasts $\bar{\mathbf{w}}_c^{(t)}$ across its subnet. The devices subsequently obtain their final updated models with local aggregation as $\mathbf{w}_i^{(t)} = \bar{\mathbf{w}}_c^{(t)}, i \in \mathcal{S}_c$.

Based on the above described procedure, we can obtain the following general local model update rule at each device $i \in \mathcal{S}_c$:

$$\mathbf{w}_i^{(t)} = (1 - \Theta_c^{(t)})\tilde{\mathbf{w}}_i^{(t)} + \Theta_c^{(t)}\bar{\mathbf{w}}_c^{(t)}, \quad \forall t \in \mathcal{T}_k, \quad (13)$$

where $\Theta_c^{(t)}$ is the indicator of local model aggregation, defined as

$$\Theta_c^{(t)} = \begin{cases} 0, & t \in \mathcal{T}_k \setminus \mathcal{T}_{k,c}^L \\ 1, & t \in \mathcal{T}_{k,c}^L. \end{cases} \quad (14)$$

Communication Delay and Global Model Aggregations: In this work, we explicitly consider the communication delay from the edge to the cloud during model training. During global aggregation k , the upstream communication delay of local models from devices to the main server is denoted as Δ_k^U , while the downstream delay of the global model to edge devices is denoted as Δ_k^D . We then introduce the *round-trip communication delay* to describe the duration from the moment edge devices transmit their local models to the edge servers (which subsequently forward them to the main server) until the devices finalize their local model synchronization using the received global model, expressed as $\Delta_k = \Delta_k^U + \Delta_k^D$, assuming $0 \leq \Delta_k \leq \tau_k - 1$, $\forall k$. Both uplink Δ_k^U and downlink delay Δ_k^D are quantified in terms of the *number* of local SGD update rounds that edge devices can perform during this period.

In conducting global aggregations, to account for the round-trip delay, devices send their local models to the edge servers Δ_k time instances prior to the completion of each local model training interval \mathcal{T}_k , i.e., $t = t_{k+1} - \Delta_k \in \mathcal{T}_k$. Concurrently, these devices carry out an additional Δ_k local updates using local model updates before they receive the updated global model. We assume that Δ_k can be reasonably estimated, e.g., from round-trip delays observed in recent time periods⁴

The edge servers then forward the locally aggregated models $\bar{\mathbf{w}}_c^{(t)}$ to the main server with the delay of Δ_k^U . The main server builds the global model based on the *stale* local models as

$$\bar{\mathbf{w}}^{(t)} = \sum_{c=1}^N \varrho_c \bar{\mathbf{w}}_c^{(t)}, \quad t = t_{k+1} - \Delta_k, k = 0, 1, \dots, \quad (15)$$

where $\bar{\mathbf{w}}^{(t)} = \sum_{c=1}^N \varrho_c \bar{\mathbf{w}}_c^{(t)}$ is the global average of local models for all t and ϱ_c is defined in (3). Note that the computation of the global model $\bar{\mathbf{w}}^{(t_{k+1}-\Delta_k)}$ is performed by the main server at

⁴In this study, we utilize the most recently observed delay, measured during the last local model training interval, as an approximation for the forthcoming round-trip delay, drawing inspiration from TCP analysis where round-trip times remain fairly stable for tens of seconds [38].

Algorithm 1: Delay-aware federated learning DFL with set control parameters.

Input: Length of training T , number of global aggregations K , local aggregation instances $\mathcal{T}_{k,c}^L, c = 1, \dots, N$, length of local model training intervals $\tau_k, \forall k$, combiner weights $\alpha_k, \forall k$, learning rates $\eta_k, \forall k$, minibatch sizes $|\xi_i^{(t)}|, i \in \mathcal{I}, \forall t$

Output: Final global model $\bar{\mathbf{w}}^{(T)}$

```

1 // Initialization by the server
2 Initialize  $\bar{\mathbf{w}}^{(0)}$  and broadcast it across edge devices, resulting in  $\mathbf{w}_i^{(0)} = \bar{\mathbf{w}}^{(0)}, i \in \mathcal{I}$ .
3 for  $k = 0 : K - 1$  do
4     for  $t = t_k + 1 : t_{k+1}$  do
5         for  $c = 1 : N$  do // Procedure at each subnet  $\mathcal{S}_c$ 
6             Local SGD update with:  $\tilde{\mathbf{w}}_i^{(t)} = \mathbf{w}_i^{(t-1)} - \eta_{t-1} \hat{\mathbf{g}}_i^{(t-1)}$ ;
7             if  $t \in \mathcal{T}_{k,c}^L$  then
8                 Local model aggregation with:  $\bar{\mathbf{w}}_c^{(t)} = \sum_{i \in \mathcal{S}_c} \rho_{i,c} \tilde{\mathbf{w}}_i^{(t)}$  and  $\mathbf{w}_i^{(t)} = \bar{\mathbf{w}}_c^{(t)}$ ;
9             else
10                 $\mathbf{w}_i^{(t)} = \tilde{\mathbf{w}}_i^{(t)}$ .
11            end
12        end
13        if  $t = t_{k+1} - \Delta_k$  then
14            for  $c = 1 : N$  do // Procedure at each subnet  $\mathcal{S}_c$ 
15                Local model aggregation:  $\bar{\mathbf{w}}_c^{(t)} = \sum_{i \in \mathcal{S}_c} \rho_{i,c} \tilde{\mathbf{w}}_i^{(t)}$  and uplink transmission.
16            end
17        else if  $t = t_{k+1} - \Delta_k^D$  then // Procedure at main server
18            Global model aggregation:  $\bar{\mathbf{w}}^{(t_{k+1}-\Delta_k)} = \sum_{c=1}^N \varrho_c \bar{\mathbf{w}}_c^{(t_{k+1}-\Delta_k)}$  and downlink broadcast.
19        else if  $t = t_{k+1}$  and  $t \neq T$  then // Procedure at each cluster  $\mathcal{S}_c$ 
20            Local-Global model combiner:  $\mathbf{w}_i^{(t)} = (1 - \alpha_k) \bar{\mathbf{w}}^{(t-\Delta_k)} + \alpha_k \left( (1 - \Theta_c^{(t)}) \tilde{\mathbf{w}}_i^{(t)} + \Theta_c^{(t)} \sum_{j \in \mathcal{S}_c} \rho_{j,c} \tilde{\mathbf{w}}_j^{(t)} \right)$ .
21        end
22    end
23 end

```

$t = t_{k+1} - \Delta_k^D$. After the computation at the main server, the global model $\bar{\mathbf{w}}^{(t_{k+1}-\Delta_k)}$ is then broadcast and received at the devices with the delay of Δ_k^D . The devices then synchronize their local models at time t_{k+1} via a linear local-global model combiner, as follows.

Linear Local-Global Model Combiner (Global Synchronization): The conventional rule for updating the local model in FL is to synchronize based on the global model, i.e., $\mathbf{w}_i^{(t_k)} = \bar{\mathbf{w}}^{(t_{k+1}-\Delta_k)}$. However, in our setting, the devices have conducted Δ_k more local updates before receiving the global model, which this standard synchronization would effectively neglect, resulting in synchronizing the local model with stale global model $\bar{\mathbf{w}}^{(t_{k+1}-\Delta_k)}$. To address this, we propose a linear global-local model combiner scheme in which each edge device i updates its local model based on the received global model at time t_{k+1} as

$$\mathbf{w}_i^{(t_{k+1})} = (1 - \alpha_k) \bar{\mathbf{w}}^{(t_{k+1}-\Delta_k)} + \alpha_k \left((1 - \Theta_c^{(t_{k+1})}) \tilde{\mathbf{w}}_i^{(t_{k+1})} + \Theta_c^{(t_{k+1})} \sum_{j \in \mathcal{S}_c} \rho_{j,c} \tilde{\mathbf{w}}_j^{(t_{k+1})} \right), \forall i \in \mathcal{I}, \quad (16)$$

where $\alpha_k \in [0, 1)$ is the *combiner weight* employed in update iteration k , with $\alpha_k = 0$ corresponding to the conventional synchronization rule. Devices will then commence their local SGD iterations over \mathcal{T}_{k+1} initialized based on (16). Intuitively, α_k should be carefully tuned to compensate for the tradeoff between the *staleness* of the global model and the potential for local model *overfitting* to each device's dataset. In particular, when we have a larger delay Δ_k , α_k is expected to be larger since the global model received will be based on more outdated local models. In Sec. IV, we will develop a control algorithm (i.e., Algorithm 2) to determine τ_k and α_k given round-trip delay Δ_k for each local model training interval.

The pseudocode for the DFL algorithm with preset control parameters is given in Algorithm 1. In Section IV, we present the corresponding control algorithm (Algorithm 2) that tunes the algorithm parameters to achieve a sublinear convergence rate based on the bound derived in Sec. III, while mitigating network costs.

III. CONVERGENCE ANALYSIS OF DFL

In this section, we aim to provide a theoretical analysis of the convergence behavior of the global deployed model under DFL. To facilitate this analysis, we adopt an approach similar to [39]. We break down the errors between the local models and the global optimum into: 1) the error between the local models and *virtual* models following noise-free dynamics; and 2) the errors between the latter and the global optimum. To this end, we define a virtual subnet *noise-free variable* (i.e., it considers the full-batch gradient of $\bar{F}_c(\cdot)$, thereby neglecting the SGD noise and intra-subnet diversity) that remains constant throughout the entire training period as

$$\bar{\mathbf{v}}_c^{(t+1)} = \bar{\mathbf{v}}_c^{(t)} - \eta_k \nabla \bar{F}_c(\bar{\mathbf{v}}_c^{(t)}), \quad \forall t \in \mathcal{T}_k \setminus \{t_k\}. \quad (17)$$

The *subnet noise-free variable at global synchronization* is defined as

$$\bar{\mathbf{v}}_c^{(t_{k+1})} = (1 - \alpha_k) \bar{\mathbf{v}}_c^{(t_{k+1} - \Delta_k)} + \alpha_k \tilde{\mathbf{v}}_c^{(t_{k+1})}, \quad (18)$$

where $\tilde{\mathbf{v}}_c^{(t_{k+1})}$ is the noise-free variable right before global synchronization, as opposed to $\mathbf{v}_c^{(t_{k+1})}$ defined immediately after global synchronization. Similarly, we define the *virtual global noise-free variable* as

$$\bar{\mathbf{v}}^{(t+1)} = \sum_{d=1}^N \varrho_d \bar{\mathbf{v}}_d^{(t+1)}, \quad \forall t \in \mathcal{T}_k. \quad (19)$$

To simplify the presentation of the convergence analysis, we assume $\alpha_k = \alpha$ (i.e., the weighing coefficient in (18)) $\tau_k = \tau$ (i.e., the length of local model training interval) and $\Delta_k = \Delta$ (i.e., the

delay), are constants throughout the training, for all k . This matches the design of the control algorithm presented in Algorithm 2 (Sec. IV), where an optimization formulation is formulated at the beginning of each global synchronization to optimize the performance metrics of our interest for the remaining of ML model training time and determine τ_k and α_k for each aggregation given the edge-to-cloud communication delay Δ_k . Although α , τ , and Δ are assumed to be fixed in the convergence analysis, we will later use the analysis results to obtain instantaneous α_k for DFL.

A. Intermediate Quantities and Results

We make the following assumptions and define three quantities used throughout the analysis.

Assumption 2 (SGD Noise Characteristics). *Let $\mathbf{n}_i^{(t)} = \widehat{\mathbf{g}}_i^{(t)} - \nabla F_i(\mathbf{w}_i^{(t)}) \forall i, t$ denote the noise of the estimated gradient through the SGD process for device i at time t . The conditional expectation based on time t is $\mathbb{E}_t[\mathbf{n}_i^{(t)}] = \mathbf{0}$ with an upper bound σ^2 on the variance of the noises, such that $\exists \sigma > 0 : \mathbb{E}_t[\|\mathbf{n}_i^{(t)}\|^2] \leq \sigma^2, \forall i, t$.*

Assumption 3 (Subnet Deviation Noise). *We assume that $\Theta_c^{(t)}$ is chosen such that the following noise within a subnet is upper bounded by ϕ^2*

$$\sum_{c=1}^N \varrho_c (1 - \Theta_c^{(t)}) (2\delta_c^2 + 4\omega_c^2 \beta^2 \|\bar{\mathbf{v}}_c^{(t)} - \mathbf{w}^*\|^2) \leq \phi^2, \quad (20)$$

where $\phi > 0$ is a constant.

We will ensure the enforcement of the above assumption through the control algorithm in Sec. IV. We now define the following set of error terms.

1) *Subnet Deviation Error:* We define the *subnet deviation error* as follows:

$$e_1^{(t+1)} \triangleq \mathbb{E} \left[\sum_{c=1}^N \varrho_c \sum_{j \in \mathcal{S}_c} \rho_{j,c} \|\mathbf{w}_j^{(t+1)} - \bar{\mathbf{v}}_c^{(t+1)}\|^2 \right]^{1/2}. \quad (21)$$

$e_1^{(t)}$ captures the average deviation error of local models of devices within a subnet from the subnet noise-free variable.

2) *Expected Model Dispersion and Optimality Gap of the Noise-Free Variable:* We next define

$$e_2^{(t)} = \sum_{c=1}^N \varrho_c \mathbb{E} [\|\bar{\mathbf{v}}_c^{(t)} - \bar{\mathbf{v}}^{(t)}\|] \quad (22)$$

as the *expected model dispersion* of the noise-free variable with $\bar{\mathbf{v}}_c^{(t)}$ and $\bar{\mathbf{v}}^{(t)}$ defined in (17) and (19) respectively. $e_2^{(t)}$ measures the degree to which the subnet noise-free variable deviates from the global noise-free variable during the local model training interval. In addition, we define

$$e_3^{(t)} = \mathbb{E}[\|\bar{\mathbf{v}}^{(t)} - \mathbf{w}^*\|] \quad (23)$$

as the *expected optimality gap of the Noise-Free variable*. $e_3^{(t)}$ measures the degree to which the global noise-free variable deviates from the optimum during the local model training interval.

Obtaining a general upper bound on $e_2^{(t)}$ and $e_3^{(t)}$ is non-trivial due to the coupling between the gradient diversity and the model parameters imposed by (7) and (8). For an appropriate choice of step size in (11), we upper bound these quantities by analyzing coupled variable systems. Upper bounds of $e_1^{(t)}$, $e_2^{(t)}$ and $e_3^{(t)}$ are illustrated in the following Lemma and Proposition. Using these bounds, we later obtain the convergence bounds of the global deployed model obtained in DFL.

Lemma 1 (One-step behavior of $e_1^{(t)}$, $e_2^{(t)}$ and $e_3^{(t)}$). *For $t \in \mathcal{T}_k$ before performing global synchronization, under Assumptions 1, 2 and 3, if $\eta_k \leq \frac{2}{\mu+\beta}$, $\forall k$, using DFL for ML model training, in $t \in \mathcal{T}_k$, the one-step behaviors of $(e_1^{(t+1)})^2$, $e_2^{(t+1)}$ and $e_3^{(t+1)}$ are presented as follows:*

$$(e_1^{(t+1)})^2 \leq (1 - \mu\eta_k)^2 (e_1^{(t)})^2 + \eta_k^2 (\sigma^2 + \phi^2), \quad (24)$$

$$e_2^{(t+1)} \leq (1 + \eta_k(\beta - \mu))e_2^{(t)} + 2\omega\eta_k\beta e_3^{(t)} + \eta_k\delta, \quad (25)$$

$$e_3^{(t+1)} \leq (1 - \eta_k\mu)e_3^{(t)} + \eta_k\beta e_2^{(t)}. \quad (26)$$

Lemma 1 characterizes the one-step dynamics of $e_1^{(t)}$, $e_2^{(t)}$, and $e_3^{(t)}$ within a local model training interval. During local model updates, the upper bounds of $e_1^{(t)}$ and $e_3^{(t)}$ display a contraction behavior among different terms, while the upper bound of $e_2^{(t)}$ exhibits a monotonic increase. Given that the upper bounds for $e_2^{(t)}$ and $e_3^{(t)}$ are interrelated, it is essential to investigate their mutual impact and the role of the combiner weight in shaping their behavior at the global synchronization stage. This investigation will be conducted in the subsequent proposition.

Proposition 1 (Upper bounds for $e_1^{(t_{k+1})}$, $e_2^{(t_{k+1})}$ and $e_3^{(t_{k+1})}$). *Under Assumptions 1, 2 and 3, if $\eta_k = \frac{\eta_{\max}}{1+\gamma k}$, where $\eta_{\max} < \min \left\{ \frac{2}{\beta+\mu}, \frac{(\tau-\Delta)\mu}{\beta^2[(1+\lambda_+)^{\tau-1}-\tau\lambda_+]} \right\}$, there exists constants C_1 , C_2 , C_3 , K_1 , K_2 and λ_{\pm} such that $(e_1^{(t_{k+1})})^2$, $e_2^{(t_{k+1})}$ and $e_3^{(t_{k+1})}$ across global synchronizations in DFL can be bounded as*

$$(e_1^{(t_{k+1})})^2 \leq (1 - \eta_k/\eta_{\max}C_1) (e_1^{(t_k)})^2 + \eta_k^2 (\tau - (1 - \alpha)\Delta) (\sigma^2 + \phi^2), \quad (27)$$

$$e_2^{(t_{k+1})} \leq \alpha(1 + \lambda_+)^{\tau} e_2^{(t_k)} + \eta_k \alpha 2\omega C_2 e_3^{(t_k)} + \eta_k \alpha K_1 \delta, \quad (28)$$

$$e_3^{(t_{k+1})} \leq (1 - \eta_k \beta C_3) e_3^{(t_k)} + C_2 \eta_k e_2^{(t_k)} + \eta_k^2 K_2 \delta, \quad (29)$$

where the expressions of the constants are provided in Appendix B.

Sketch of Proof: The complete proof is provided in Appendix B. To prove Proposition 1, we first use Lemma 1 to derive the one-step dynamics of $e_1^{(t+1)}$, $e_2^{(t+1)}$, and $e_3^{(t+1)}$ across the local model training period. Next, we apply the one-step dynamics from Lemma 1 repeatedly to solve the coupled dynamics and obtain the recurrence relationship of $e_1^{(t_{k+1})}$, $e_2^{(t_{k+1})}$, and $e_3^{(t_{k+1})}$ across the global synchronization periods as follows:

$$(e_1^{(t_{k+1})})^2 \leq [(1 - \alpha)(1 - \mu\eta_k)^{2(\tau - \Delta)} + \alpha(1 - \mu\eta_k)^{2\tau}] (e_1^{(t_k)})^2 + [\tau - (1 - \alpha)\Delta] \eta_k^2 (\sigma^2 + \phi^2), \quad (30)$$

$$e_2^{(t_{k+1})} \leq \alpha \Pi_{+,t_{k+1}} e_2^{(t_k)} + \alpha \frac{4\omega}{\sqrt{8\omega + 1}} [\Pi_{+,t_{k+1}} - 1] e_3^{(t_k)} + \alpha \frac{\mu}{-\beta^2 \lambda_+ \lambda_-} [\Pi_{+,t_{k+1}} - 1] \delta, \quad (31)$$

$$\begin{aligned} e_3^{(t_{k+1})} &\leq \Psi_1(\eta_k) e_3^{(t_k)} + \underbrace{2g_3[(1 - \alpha)\Pi_{+,t_{k+1} - \Delta} + \alpha\Pi_{+,t_{k+1}} - 1]}_{(a)} e_2^{(t_k)} \\ &+ \underbrace{[(1 - \alpha)[g_5(\Pi_{+,t_{k+1} - \Delta} - 1) + g_6(\Pi_{-,t_{k+1} - \Delta} - 1)] + \alpha[g_5(\Pi_{+,t_{k+1}} - 1) + g_6(\Pi_{-,t_{k+1}} - 1)]}_{(b)} \delta / \beta \end{aligned} \quad (32)$$

with the expression of $\Psi_1(\cdot)$, g_3 , g_5 , g_6 , and $\Pi_{\{+,-\},t} = [1 + \eta_k \beta \lambda_{\{+,-\}}]^{t-t_k}$ provided in Lemma 2 in Appendix C. Utilizing the convexity of $[(1 - \alpha)(1 - \mu\eta_k)^{2(\tau - \Delta)} + \alpha(1 - \mu\eta_k)^{2\tau}]$ in (30) and $\Pi_{+,t_{k+1}}$ (31), we are able to derive the bounds presented in (27) and (28). Finally, considering (32), we bound $\Psi_1(\eta_k)$ as follows: Since $\lambda_- \leq \lambda_+$, $\eta_k \leq \eta_{\max}$ and $\eta_k \beta \leq 1$, we apply the binomial theorem along with a set of algebraic manipulations to get

$$\frac{\Psi_1(\eta_k) - 1}{\eta_k \beta} \leq -(\tau - \Delta) \mu / \beta + \eta_{\max} \beta [(1 + \lambda_+)^{\tau} - 1 - \tau \lambda_+] \triangleq -C_3, \quad (33)$$

and therefore $\Psi_1(\eta_k) \leq 1 - \eta_k \beta C_3 < 1$. We then proceed by bounding (a) in (32). Using the convexity of $\Pi_{+,t} - 1$ with respect to both $\eta_k \beta$ and $\eta_{\max} \beta$ with the constraint $\eta_{\max} \beta \leq 1$, we obtain $2g_3[(1 - \alpha)\Pi_{+,t_{k+1} - \Delta} + \alpha\Pi_{+,t_{k+1}} - 1] \leq \eta_k C_2$. Finally, we bound (b) in (32), using the binomial expansion and the expressions of g_5 and g_6 , which yields $g_5(\Pi_{+,t} - 1) + g_6(\Pi_{-,t} - 1) \leq \eta_k^2 \beta K_2$. Replacing these bounds in (32) leads to the final result in (29). \blacksquare

Proposition 1 provides insight about the impact of subnets on the convergence of model training by bounding the subnet deviation error $(e_1^{(t_{k+1})})^2$ in (27). It shows that $(e_1^{(t_{k+1})})^2$ is (i)

dependent on the optimality gap of the subnet error-free variable (i.e., $\mathbb{E}[\|\bar{\mathbf{v}}_c^{(t)} - \mathbf{w}^*\|^2]$, $\forall t \in \mathcal{T}_k$ encapsulated in ϕ), (ii) sensitive to SGD noise and intra-subnet data diversity encapsulated in ϕ (the bound increases as σ , δ_c and ω_c increase), and (iii) getting larger as the period of local aggregation (i.e., t_k^L) increases. To demonstrate the convergence of $(e_1^{(t_{k+1})})^2$, it is necessary to ensure Assumption 3 is satisfied by monitoring the dynamic of $\mathbb{E}[\|\bar{\mathbf{v}}_c^{(t)} - \mathbf{w}^*\|^2]$ and selecting appropriate local aggregation instances $\{\Theta_c^{(t)}\}_{t \in \mathcal{T}_k}$. Our control algorithm in Sec. IV demonstrates how this can be achieved. Proposition 1 also reveals the evolution of $e_2^{(t_k)}$ and $e_3^{(t_k)}$ across global synchronizations. The bounds (28) and (29) demonstrate that $e_2^{(t_k)}$ and $e_3^{(t_k)}$ are (i) interdependent, forming a coupled relationship, and (ii) influenced by the inter-subnet data diversity (the bounds increase as δ increases for a fixed value of ω). The bound in (28) also establishes a necessary condition for the combiner weight α to exhibit a contraction behavior during training. In particular, to achieve this behavior, α must be strictly less than $\frac{1}{(1+\lambda_+)\tau}$. This condition is crucial for DFL to achieve convergence and will be further used in Theorem 1.

B. General Convergence Behavior of DFL

Using the aforementioned results, we will next demonstrate that the global model deployed under DFL can achieve sublinear convergence to the optimum model.

Theorem 1 (Sublinear Convergence of DFL). *Under Assumptions 1, 2 and 3, if $\eta_k = \frac{\eta_{\max}}{1+\gamma_k}$, $\forall k$ and $|\mathcal{T}_k| \leq \tau$, $\forall k$, there exists constants Y_1 , Y_2 and Y_3 such that the distance between the global model and the optimal model at each global synchronization in DFL can be bounded as*

$$\mathbb{E}[\|\bar{\mathbf{w}}^{(t_k)} - \mathbf{w}^*\|^2] \leq \underbrace{2Y_1^2\eta_k}_{(a)} + \underbrace{2Y_3^2\eta_k^2}_{(b)}, \quad (34)$$

where $\eta_{\max} < \min \left\{ \frac{2}{\beta+\mu}, \frac{(\tau-\Delta)\mu}{\beta^2[(1+\lambda_+)\tau-1-\tau\lambda_+]} \right\}$, $\gamma < \min \{1 - (1 - \mu\eta_{\max})^{2(\tau-\Delta)}, C_3\eta_{\max}\beta\}$,

$$\alpha < \alpha^* \triangleq \frac{1}{\frac{C_2\eta_{\max}^2}{\eta_{\max}\beta C_{3-\gamma}} 2\omega C_2(1+\gamma) + (1+\gamma)(1+\lambda_+)\tau}, \quad (35)$$

with the expression of the constants provided in Appendix A.

Sketch of Proof: The complete proof is provided in Appendix A. We first obtain that

$\sqrt{\mathbb{E}[\|\bar{\mathbf{w}}^{(t_k)} - \mathbf{w}^*\|^2]} \leq e_1^{(t_k)} + e_3^{(t_k)}$, and thus

$$\mathbb{E}[\|\bar{\mathbf{w}}^{(t_k)} - \mathbf{w}^*\|^2] \leq (e_1^{(t_k)} + e_3^{(t_k)})^2 \leq 2(e_1^{(t_k)})^2 + 2(e_3^{(t_k)})^2. \quad (36)$$

We will prove (34) by induction, showing that $e_1^{(t_k)} \leq Y_1\sqrt{\eta_k}$, $e_2^{(t_k)} \leq Y_2\eta_k$, and $e_3^{(t_k)} \leq Y_3\eta_k$. The base of induction trivially holds since $Y_1 \geq 0$, $Y_2 \geq 0$, and $Y_3 \geq \eta_{\max}e_3^{(0)}$ at the start of training ($k = 0$). For the induction step, assume that the statement holds true for some $k \in \mathbb{N}$. We then show that it also holds for $k + 1$. To show $e_1^{(t_{k+1})} \leq \sqrt{\eta_{k+1}}Y_1$, we use (27) and the induction hypothesis ($e_1^{(t_k)} \leq \sqrt{\eta_k}Y_1$), yielding the sufficient condition for all $k \geq 0$:

$$\eta_{\max}(\tau - (1 - \alpha)\Delta)(\sigma^2 + \phi^2) \leq [C_1 - \gamma]Y_1^2,$$

which is verified since $\gamma < 1 - (1 - \mu\eta_{\max})^{2(\tau-\Delta)} \leq C_1$ and $Y_1^2 = \frac{(\tau-(1-\alpha)\Delta)(\sigma^2+\phi^2)\eta_{\max}}{C_1-\gamma}$. Thus we can show for $e_1^{(t_k)}$ that $(e_1^{(t_k)})^2 \leq \eta_k Y_1^2$, $\forall k$. To show $e_2^{(t_{k+1})} \leq \eta_{k+1}Y_2$, we use (28) and the induction hypothesis ($e_2^{(t_k)} \leq \eta_k Y_2$), yielding

$$\alpha(1 + \lambda_+)^{\tau}\eta_k Y_2 + \alpha 2\omega C_2 \eta_k^2 Y_3 + \alpha K_1 \eta_k \delta - \eta_{k+1} Y_2 \leq 0, \quad (37)$$

To satisfy the above condition for all $k \geq 0$, it is enough to have

$$\frac{[1 - \alpha(1 + \gamma)(1 + \lambda_+)^{\tau}]Y_2 - \alpha K_1 \delta(1 + \gamma)}{\eta_{\max}} - \alpha 2\omega C_2 Y_3(1 + \gamma) \geq 0. \quad (38)$$

Holding on proving the final results of the upper bound on $e_2^{(t_{k+1})}$, we take a look at $e_3^{(t_{k+1})}$ to show $e_3^{(t_{k+1})} \leq \eta_{k+1}Y_3$. We use (29) and the induction hypothesis ($e_3^{(t_k)} \leq \eta_k Y_3$), yielding

$$(1 - \eta_k \beta C_3)Y_3 \eta_k + [C_2 Y_2 + K_2 \delta] \eta_k^2 - Y_3 \eta_{k+1} \leq 0. \quad (39)$$

The above condition is equivalent to satisfying the following condition for all $k \geq 0$:

$$Y_3[\gamma - \eta_{\max}\beta C_3] + [C_2 Y_2 + K_2 \delta] \eta_{\max} \leq 0. \quad (40)$$

To demonstrate $e_2^{(t_k)} \leq \eta_{k+1}Y_2$ and $e_3^{(t_k)} \leq \eta_{k+1}Y_3$, it is necessary that conditions $e_3^{(t_k)} \geq \eta_{\max}e_3^{(0)}$, (38), and (40) hold simultaneously, which can be achieved by noting that $\alpha < \alpha^*$ and utilizing the definition of Y_2 in (52). Completing the induction, we show that $e_2^{(t_k)} \leq \eta_{k+1}Y_2$ and $e_3^{(t_k)} \leq \eta_{k+1}Y_3$. Finally, substituting these results back into (36) completes the proof. ■

Investigating the bound in (34) of Theorem 1, we found conditions for DFL to achieve a convergence rate of $\mathcal{O}(1/t)$. Note that the decay rate of (a) is faster than (b) across global synchronizations, indicating that the impact of inter-gradient diversity (i.e., ω and δ) incorporated into Y_3 on the bound decays faster than that of intra-gradient diversity incorporated into Y_1 . The bound also demonstrates the effect of the combiner weight α on convergence. In particular, when $\Delta = 0$, the optimal choice of α is the trivial solution (i.e., $\alpha = 0$ since this choice leads to minimizing Y_3), indicating that it is optimal for DFL to perform the standard FedAvg

algorithm without local-global model combination. Given a fixed value of ω , as the gradient diversity (i.e., δ) increases, it becomes more favorable to choose a smaller value of α to achieve better convergence, demonstrating the importance of putting a higher importance on the global model during local-global model combination to avoid having biased local models under data heterogeneity. The value of the bound increases with respect to the subnet deviation noise (i.e., ϕ), implying that DFL can achieve the same performance under less frequent global aggregations with more frequent local aggregations. This further suggests that the local model training interval can be prolonged upon performing more rounds of local aggregations in between global aggregations. Moreover, the convergence bound shows the non-triviality of selecting α for the best convergence behavior (as discussed in Sec. IV).

In the next section, we will leverage these relationships in developing an adaptive control algorithm for DFL that tunes the algorithm parameters to achieve the convergence bound in Theorem 1 while reducing the network costs.

IV. ADAPTIVE CONTROL ALGORITHM FOR DFL

In this section, we develop a control algorithm based on Theorem 1 for tuning the controllable parameters in DFL, while guaranteeing the sublinear convergence of the model. In DFL, there are four sets of controllable parameters: (i) local model training intervals $\{\tau_k\}$, (ii) the combiner weight $\{\alpha_k\}$, (iii) the gradient descent step size $\{\eta_k\}$, and (iv) the instances of local aggregations $\{\mathcal{T}_{k,c}^L\}$. The decisions on (i), (ii), (iii) and (iv) are made by the main server at $t = t_{k+1} - \Delta_k^D$, $\forall k$ during global aggregation.

To tune these parameters, we develop a control algorithm consisting of the following two parts. *Part I*: an adaptive technique (Sec. IV-A) to determine the step-size (i.e., η_{max} and γ in η_k defined in Theorem 1) considering the conditions imposed by Theorem 1. *Part II*: an optimization scheme (Sec. IV-B) to tune τ_k and α_k accounting for the tradeoff between the ML model performance and network resource consumption. In Sec. IV-C, we provide the pseudocode summarizing how Parts I and II are integrated.

A. Step Size Parameters (η_{max} , γ)

We first tune the step size parameters (η_{max} , γ). This is done for a given set of model-related parameters ($\beta, \mu, \zeta, \delta, \zeta_c, \delta_c, \sigma, \omega$ and ω_c), which can be estimated by the server (e.g., see Sec. IV-C of [26]). Given the fact that larger feasible values of η_{max} result in larger values of step

size and thus faster convergence, given the conditions mentioned in the statement of Theorem 1, we first determine the largest value for η_{max} such that $\eta_{max} < \min \left\{ \frac{2}{\beta+\mu}, \frac{(\tau-\Delta)\mu}{\beta^2[(1+\lambda_+)^{\tau-1}-\tau\lambda_+]} \right\}$, where λ_+ is defined in Theorem 1. Afterward, we arbitrarily choose the value of γ such that $\gamma < \min \{1 - (1 - \mu\eta_{max})^{2(\tau-\Delta)}, C_3\eta_{max}\beta\}$.

We next introduce the optimization formulation to determine the length of local model training interval τ_k and the combiner weight α_k for each local model training interval.

B. Length of Local Training Interval $\{\tau_k\}$ and Value of Combiner Weight $\{\alpha_k\}$

Considering the convergence goal of DFL (i.e., sublinear convergence with low resource consumption across edge devices), we formulate an optimization problem \mathcal{P} solved by the main server at each instance of global aggregation at $t = t_k - \Delta_{k-1}^D$, $\forall k$ to tune τ_k and α_k for the subsequent local model training intervals \mathcal{T}_k , $\forall k$. The objective function of \mathcal{P} accounts for the joint impact of three metrics: (a) energy consumption of local and global model aggregation, (b) communication delay of local and global aggregation, and (c) the performance of global deployed model captured by the optimality gap in Theorem 1.

$$\begin{aligned}
 (\mathcal{P}) : \quad & \min_{\tau, \alpha} c_1 \underbrace{\left(\frac{T-t_k}{\tau} \right) \left(E_{\text{GlobAgg}} + \sum_{c=1}^N |\mathcal{A}_{\{c,k\}}| E_{c,\text{LocalAgg}} \right)}_{(a)} + \\
 & c_2 \underbrace{\left(\frac{T-t_k}{\tau} \right) \left(\Delta_{\text{GlobAgg}} + \sum_{c=1}^N |\mathcal{A}_{\{c,k\}}| \Delta_{c,\text{LocAgg}} \right)}_{(b)} + c_3 \underbrace{\nu(\tau, \alpha)}_{(c)} \\
 & \text{s.t.}
 \end{aligned}$$

$$\Delta \leq \tau \leq \min \{ \tau_{\max}, T - t_k \}, \tau_k \in \mathbb{Z}^+, \quad (41)$$

$$\alpha < \frac{1}{\frac{C_2 \eta_{\max}^2}{\eta_{\max} \beta C_3 - \gamma} 2\omega C_2 (1 + \gamma) + (1 + \gamma)(1 + \lambda_+)^{\tau}}, \quad (42)$$

where $E_{c,\text{LocalAgg}} = \sum_{j \in \mathcal{S}_c} M \times Q \times p_j / R_j^{(t)}$ is the energy consumption of conducting local model aggregation at edge server n_c , where M denotes the size of the model (i.e., number of model parameters), Q denotes the number of bits used to represent each model parameter, which is dependent on the quantization level, p_j denotes the transmit power of device $j \in \mathcal{S}_c$, and $R_j^{(t)} = W \log_2 \left(1 + \frac{p_j |h_j^{(t)}|^2}{N_0 W} \right)$ is the transmission rate between device $j \in \mathcal{S}_c$ and its associated edge server n_c at time t . The noise power is $N_0 W$, with N_0 as the white noise power spectral density, W as the

bandwidth, and $h_j^{(t)}$ as the channel coefficient. $E_{\text{GlobAgg}} = \sum_{n_c \in \mathcal{N}} M \times Q \times \bar{p}_{n_c} / \bar{R}_{n_c}^{(t)}$ is the energy consumption for edge-to-main server communications, where \bar{p}_{n_c} and $\bar{R}_{n_c}^{(t)}$ denote the transmit power of edge server n_c and the transmission rate between the edge server $n_c \in \mathcal{N}$, $\forall c$ and the main server, respectively. Furthermore, $\Delta_{\text{c,LocalAgg}} = \max_{j \in \mathcal{S}_c} \{M \times Q / R_j^{(t)}\}$ is the communication delay of performing local aggregation via device $j \in \mathcal{S}_c$.⁵ $\Delta_{\text{GlobAgg}} = \max_{i \in \mathcal{I}} \{\Delta_k / R(\xi_i^{(t)})\}$ is the device-to-main server communication delay, where Δ_k denotes the round-trip delay measured in terms of the number of conducted SGD's and $R(\xi_i^{(t)})$ denotes the processing rate (the number of SGD's conducted at each time instance measured in seconds) at edge device i .

In \mathcal{P} , $|\mathcal{A}_{\{c,k\}}|$ is the number of local aggregations performed by devices $i \in \mathcal{S}_c$ within a period of local model training interval, which we obtain as $\mathcal{A}_{\{c,k\}} = \{t \in \mathcal{T}_k : \sum_{c=1}^N \varrho_c(1 - \Theta_c^{(t)})(2\delta_c^2 + 4\omega_c^2\beta^2\|\bar{\mathbf{v}}_c^{(t)} - \mathbf{w}^*\|^2) > \phi^2\}$ (see Assumption 3). To obtain $\mathcal{A}_{\{c,k\}}$ we thus need to control $\|\bar{\mathbf{v}}_c^{(t)} - \mathbf{w}^*\|^2$, to monitor the value of which, we first approximate it as $\|\bar{\mathbf{v}}_c^{(t)} - \mathbf{w}^*\|^2 \approx \|\bar{\bar{\mathbf{w}}}_c^{(t)} - \mathbf{w}^*\|^2$. Then, during each local aggregation, the edge server estimates the upper bound on $\|\bar{\bar{\mathbf{w}}}_c^{(t)} - \mathbf{w}^*\|^2$ using strong convexity of $F(\cdot)$ (i.e., $\|\nabla F(\bar{\bar{\mathbf{w}}}_c^{(t)})\|^2 \geq \mu^2\|\bar{\bar{\mathbf{w}}}_c^{(t)} - \mathbf{w}^*\|^2$). Finally, $\nu(\tau, \alpha) = 2Y_1^2\eta_K + 2Y_3^2\eta_K^2$ denotes the optimality gap upper bound derived in Theorem 1 at time $t_K = T$. To compute Y_3 , we first approximate $e_3^{(0)} \approx \|\bar{\mathbf{w}}^{(0)} - \mathbf{w}^*\|$, and then estimate its using its upper bound $\|\nabla F(\bar{\mathbf{w}}^{(0)})\| \geq \mu\|\bar{\mathbf{w}}^{(0)} - \mathbf{w}^*\|$.

Constraints. The constraint in (41) guarantees that the value of τ_k is larger than the edge-to-main server communication delay, matching our assumption in Sec. II-C. Constraint (42) is a condition on α described in Theorem 1 and ensures that the value of α lies within a range to guarantee the sublinear convergence of the global deployed model.

Solution. Formulation \mathcal{P} is a non-convex mixed-integer programming problem. Due to the complex nature of the problem, we solve it via exhaustive search, performing line search over the integer values of τ in the range given in (41) and obtain the optimum of $\alpha \in (0, 1]$ corresponding to each value of τ . Note that, given a value of τ , \mathcal{P} is still non-convex with respect to α . Therefore, we discretize the search space of α and perform a line search over the discretized search space of α for each τ . Based on this approach, the search space of \mathcal{P} remains to be small due to the limited ranges/choices of τ and α (i.e., the time complexity of performing line search over τ is $\mathcal{O}(T - t_k - \Delta_{k-1})$ and the time complexity of performing line search over α is $\mathcal{O}(1/S_\alpha)$, where S_α is the discretization step used to discretize $(0, 1]$ interval, resulting in a

⁵The device-to-edge server communications are assumed to occur in parallel, using multiple access techniques such as FDMA.

time complexity of $\mathcal{O}((T - t_k - \Delta_{k-1}) \times 1/S_\alpha)$. Thus, we are able to solve the problem via a reasonable precision (e.g., $S_\alpha = 0.01$) in a short duration of time (e.g., less than 3 seconds on a laptop with Intel(R) Xeon(R) Gold 6242 CPU @ 2.80GHz).

C. DFL Control Algorithm

The procedure of the DFL control algorithm is outlined in Algorithm 2, which integrates the procedures described in Sec. IV-A and IV-B.

Algorithm 2: DFL with adaptive control parameters.

Input: Desirable subnet deviation error coefficient ϕ , length of model training T

Output: Global model $\bar{\mathbf{w}}^{(T)}$

```

1 Initialize  $\bar{\mathbf{w}}^{(0)}$  and broadcast it among the edge devices through the edge server.
2 Initialize estimates of  $\zeta \ll 2\beta, \delta, \sigma$ .
3 Initialize  $\eta_{max} < \min \left\{ \frac{2}{\beta+\mu}, \frac{(\tau-\Delta)\mu}{\beta^2[(1+\lambda_+)^{\tau-1}-\tau\lambda_+]} \right\}$  and  $\gamma$  for the step size  $\eta_k = \frac{\eta_{max}}{1+\gamma k}$  according to Sec. IV-A.
4 Initialize  $t = 0, k = 0, t_0 = 0, t_1 = \tau_0$ , with  $\tau_0$  chosen randomly, such that  $\tau_0 \leq T - t_k, \forall k$ .
5 while  $t \leq T$  do
6   while  $t \leq t_{k+1}$  do
7     for  $c = 1 : N$  do // Operation at the subnets
8       Each device  $i \in \mathcal{S}_c$  performs a local SGD update based on (10) and (11) using  $\mathbf{w}_i^{(t-1)}$  to obtain  $\tilde{\mathbf{w}}_i^{(t)}$ .
9       if  $t \in \mathcal{T}_{k,c}^L$  then
10         Devices inside the subnet conduct local model aggregation using (12) to obtain the updated local model  $\mathbf{w}_i^{(t)}$ .
11       else if  $t = t_{k+1}$  then
12         Devices inside each subnet perform global synchronization using (16).
13       else
14         Each device  $i \in \mathcal{S}_c$  obtains its updated local model as  $\mathbf{w}_i^{(t)} = \tilde{\mathbf{w}}_i^{(t)}$ 
15       end
16     end
17     if  $t = t_{k+1} - \Delta_k$  then // Operation at the edge server
18       Each edge server  $n_c$  sends  $\mathbf{w}_i^{(t_{k+1}-\Delta_k)}, \hat{\mathbf{g}}_i^{(t_{k+1}-\Delta_k)}, \forall i \in \mathcal{S}_c$  to the main server.
19     else if  $t = t_{k+1} - \Delta_k^D$  then // Operation at the main server
20       Compute  $\bar{\mathbf{w}}^{(t_{k+1}-\Delta_k)}$  according to (15),  $\hat{\beta}_k, \hat{\mu}_k, \hat{\sigma}_k$ .
21       Set  $\hat{\zeta}_k \ll 2\hat{\beta}_k$  and  $\hat{\zeta}_{c,k} \ll 2\hat{\beta}_k$ , then compute  $\hat{\delta}_k$  and  $\hat{\delta}_{c,k}$  using the method in [26].
22       Characterize  $\eta_{max}$  and  $\gamma$  for the step size  $\eta_k = \frac{\eta_{max}}{1+\gamma k}$  according to Sec. IV-A.
23       Compute the instances of local aggregation for each cluster  $c$  using Sec. IV-B.
24       Solve the optimization  $\mathcal{P}$  to obtain  $\tau_{k+1}$  and  $\alpha_{k+1}$ .
25       Broadcast (i)  $\bar{\mathbf{w}}^{(t_{k+1}-\Delta_k)}$ , (ii)  $\alpha_{k+1}$  and (iii)  $\eta_k$  among the devices.
26     end
27      $t \leftarrow t + 1$ 
28   end
29    $k \leftarrow k + 1$  and  $t_{k+1} \leftarrow t_k + \tau_k$ 
30 end

```

V. EXPERIMENTAL EVALUATION

This section presents numerical experiments to validate the performance of DFL. In Sec. V-A, we provide the simulation setup. Then, in Sec. V-B, we study the model training performance

and convergence behavior of DFL with set control parameters (i.e., τ_k , $\mathcal{T}_{k,c}^L$, and α_k), revealing the importance of addressing the hierarchical FL architecture and tuning the combiner weight in the presence of communication delay. In Sec. V-C, we compare the convergence behavior of our DFL control algorithm with baselines in FL [19], [40], verify our theoretical results (Sec. III-B), and illustrate the improvements in resource efficiency achieved by the DFL control algorithm.

A. System Setup

We consider a network of 50 edge devices distributed across 10 equally-sized subnets, with 5 devices per subnet. In Sec. V-C, devices within each subnet are uniformly distributed within a $30 \text{ m} \times 30 \text{ m}$ square field, and the base station is located at the center.

Communication parameters For device-to-edge wireless communications, we assume a transmission power of $p_i = 24 \text{ dBm}$ for device i , $W = 1 \text{ MHz}$ bandwidth, and $N_0 = -173 \text{ dBm/Hz}$ white noise spectral density. Fading and pathloss are modeled based on [41], using $h_i^{(t)} = \sqrt{\beta_i^{(t)}} u_i^{(t)}$, where $\beta_i^{(t)} = \beta_0 - 10\hat{\alpha} \log_{10}(d_i^{(t)}/d_0)$ is the large-scale pathloss coefficient and $u_i^{(t)} \sim \mathcal{CN}(0, 1)$ is Rayleigh fading. Here, $\beta_0 = -30 \text{ dB}$ is the pathloss at the reference distance of $d_0 = 1 \text{ m}$, $\hat{\alpha} = 3.75$ is the pathloss exponent, and $d_i^{(t)}$ is the device-to-edge server distance determined by their proximity. Channel reciprocity is assumed for simplicity. For edge-to-cloud wired communication, we employ a transmission power of $\bar{p}_{nc} = 38 \text{ dBm}$, $\bar{R}_{nc}^{(t)} = 100 \text{ Mbps}$ data rate, and a 50 ms propagation delay [37].

Computation parameters Each device's local computation time for performing each mini-batch SGD iteration on the ML model at time t can be modeled as [27] $T_{i,Comp}^{(t)} = \max_{i \in \mathcal{I}} a_i |\xi_i^{(t)}| / f_i^{(t)}$, where every device's CPU frequency is $f_i^{(t)} = 15.36 \text{ MHz}$, mini-batch size is $|\xi_i^{(t)}| = 128$ data points, and number of CPU cycles needed to process one datapoint is $a_i = 600$. The computation energy consumption of each device is modeled as $E_{i,Comp}^{(t)} = (Z_i/2) a_i B_i^{(t)} (f_i^{(t)})^2$, where the effective chipset capacitance [23] is $Z_i = 2 \times 10^{-22}$ for all devices. With these parameters, the resultant local model update processing rates are $R(\xi_i^{(t)}) = 200 \text{ updates/s}$ for all devices. In Sec. V-C3, the round-trip delay Δ_k (measured in SGD iterations) will vary according to the particular realizations generated in each round k .

We employ the Fashion-MNIST (F-MNIST) dataset for image classification, comprising samples from 10 different labels of fashion products. The dataset includes a total of 70K images, with 60K designated for training and 10K for testing. We distribute the dataset across devices in a non-i.i.d. manner such that each device has data points exclusively from s of the 10 total labels.

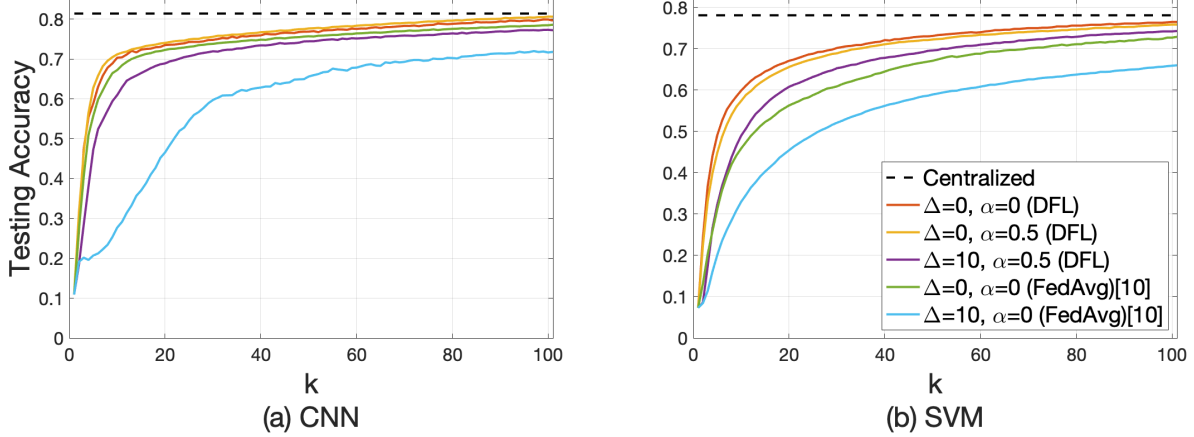


FIGURE 3: Performance comparison between DFL and standard FedAvg [10] under various choices of delay: DFL surpasses standard FedAvg with accuracy gains of 2% (CNN) and 4% (SVM) when delay is negligible ($\Delta = 0$), and further outperforms with gains of 6% (CNN) and 8% (SVM) when delay is non-negligible ($\Delta = 10$).

This results in an inherent data skewness across devices which is commonly employed to simulate non-i.i.d. settings in federated learning [22], [26], [42]. By default, we set $s = 3$. We evaluate DFL on two models: support vector machine (SVM) with regularized squared hinge loss and a convolutional neural network (CNN) with softmax and cross-entropy loss, both having model dimension $M = 7840$. This allows us to assess DFL’s performance on loss functions that are strongly convex (SVM) and those exhibiting non-convex properties (CNN).

B. DFL Model Training Performance and Convergence

We first discuss how the two major design aspects of DFL (i.e., hierarchical FL framework (Sec. V-B1) and local-global combiner (Sec. V-B2)) can affect the speed of ML model convergence and mitigate the effect of delay. We consider FedAvg [10], which performs global aggregations after each round of training with $\tau = 1$, as our benchmark. This represents an upper bound on the learning performance as it mimics centralized model training.

1) *Model convergence of hierarchical FL:* We compare the performance of DFL (Algorithm 1) with standard FedAvg model aggregation/synchronization [10]. In standard FedAvg, we consider a (hypothetical) scenario that the edge devices are directly connected to the main server. Thus the comparison would reveal the impact of hierarchical structure of DFL on model training. We consider two different scenarios: (i) when delay is negligible, and (ii) when delay is non-negligible. In scenario (i), we set the combiner weight of DFL to 0 (i.e., $\alpha = 0$) with delay $\Delta = 0$. In

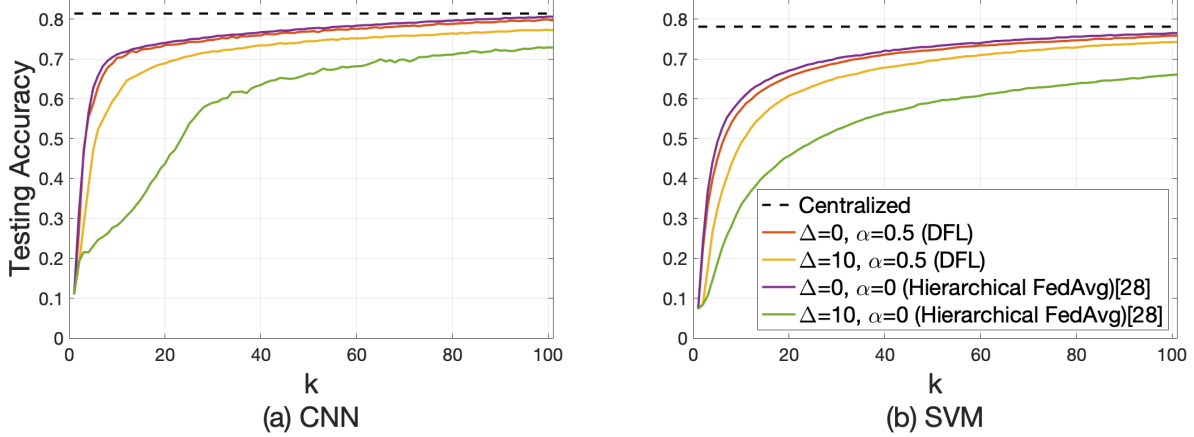


FIGURE 4: Performance comparison between DFL and hierarchical FedAvg for various α values in DFL: With $\alpha = 0.5$, DFL significantly outperforms hierarchical FedAvg when round-trip delay is $\Delta = 10$. Hierarchical FedAvg (DFL with $\alpha = 0$) performs better than DFL without delay (i.e., $\Delta = 0$), in line with Theorem 1.

scenario (ii), we set the combiner weight of DFL as $\alpha = 0.5$ with delay $\Delta = 10$. For both scenarios, DFL establishes a local model training interval $\tau_k = \tau = 20$ and performs local aggregation in the subnets after each edge device does 5 local SGD updates.

Fig. 3 validates the benefit of introducing hierarchical FL with local model aggregations by showing that DFL outperforms the standard FedAvg under both negligible and non-negligible delay. In scenarios where the delay is insignificant (i.e., $\Delta = 0$), DFL exhibits superior performance over FedAvg, achieving an accuracy gain of 2% for CNN and 4% for SVM. This highlights the benefits of a hierarchical model training structure within an edge-to-cloud network, where frequent local aggregations prevent non-i.i.d. data-driven deviation of local models from the optimum within each subnet. On the other hand, in situations where the delay is non-negligible (i.e., $\Delta = 10$), DFL outperforms FedAvg with accuracy gains of 6% for CNN and 8% for SVM. The result demonstrates the benefits of integrating the local-global combiner with the hierarchical model training architecture to account for the impact of delay.

2) *Model convergence under local-global combiner*: To further examine the efficiency enhancements provided by DFL, we conduct a comparative analysis between the performance of DFL employing a local-global combiner and the hierarchical FedAvg model as outlined in [13]–[15], [32], with both methods leveraging local aggregations. Hierarchical FedAvg can be thought of as a special case of DFL when $\alpha = 0$. DFL is executed with a fixed combiner weight of $\alpha = 0.5$, which places equal emphasis on the stale global model and up-to-date local models. The local

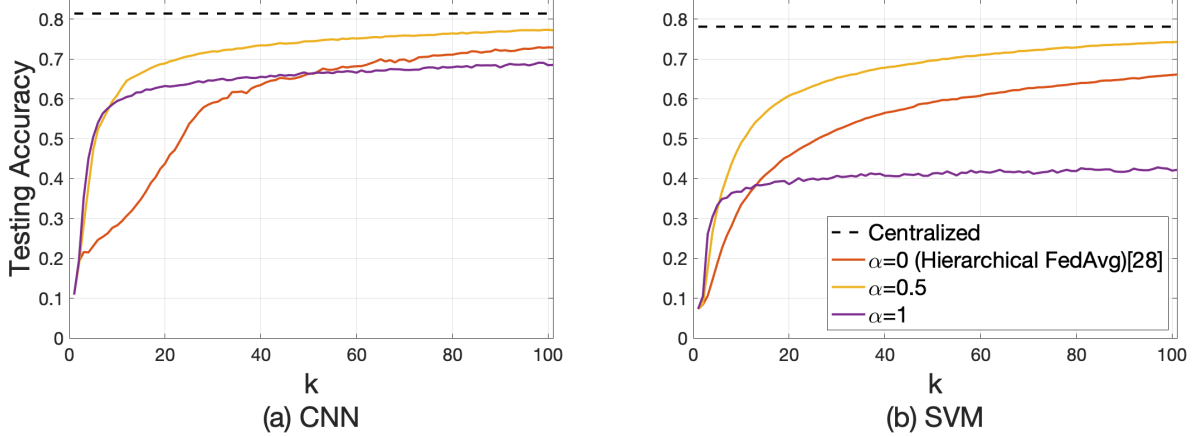


FIGURE 5: Performance comparison between DFL and hierarchical FedAvg under various choice of α in DFL under delay $\Delta = 10$. With $\alpha = 0.5$, DFL significantly outperforms hierarchical FedAvg. However, the performance of DFL was the worst with $\alpha = 0$, as no global synchronization was conducted.

model training interval is set to $\tau_k = \tau = 20$ for both DFL and hierarchical FedAvg, with a delay of $\Delta = 10$. Local aggregations are conducted after each edge device does 5 local model updates. Furthermore, we plot the convergence behavior of DFL when $\alpha = 1$, which implies that global model is never used in local devices.

Fig. 4 shows that DFL outperforms vanilla hierarchical FedAvg by utilizing the local-global combiner and achieves an accuracy gain of 5% for CNN and 8% for SVM when the delay is large (i.e., $\Delta = 10$). Conversely, Fig. 4 illustrates that when there is no delay (i.e., $\Delta = 0$), hierarchical FedAvg achieves better convergence performance than DFL, with an accuracy increase of 1% for both CNN and SVM. These findings align with the result in Theorem 1, suggesting that $\alpha = 0$ is the optimal choice of the combiner weight when $\Delta = 0$. In fact, in DFL, $\alpha = 0$ simulates the conventional hierarchical FedAvg: our results indicate that, when no delay exists ($\Delta = 0$), the best approach in DFL is to emulate hierarchical FedAvg. This validates that the conventional global aggregation procedure is indeed the most effective in the absence of delay. As the delay increases, the choice of α becomes essential and is shaped by several system variables. To highlight the robustness of DFL against delays, Fig. 4 compares its performance with hierarchical FedAvg with a negligible delay (i.e., $\Delta = 0$) as the benchmark under a non-negligible delay (i.e., $\Delta = 10$). The figure shows that even when the delay is significant, DFL achieves an accuracy within 1% and 2% of the benchmark for CNN and SVM after 100 global aggregations, demonstrating its delay-robustness. Lastly, Fig. 5 shows the convergence performance of DFL

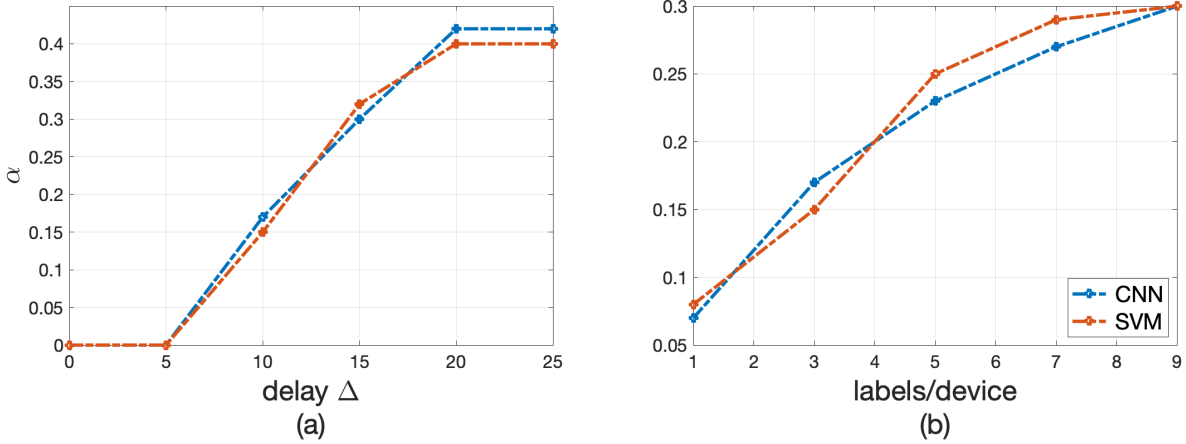


FIGURE 6: Impact of delay and data diversity on α : α increases with delay and decreases with data diversity, indicating that DFL emphasizes local models during global synchronization with high delay and global models with high data diversity.

with no usage of global model (i.e., $\alpha = 1$), where the ML model plateaus after reaching a low accuracy. This verifies the condition in Theorem 1, implying that DFL may not guarantee sublinear convergence when $\alpha = 1$.

The performance obtained by DFL originates from the introduction of the linear local-global combiner during global synchronization. This approach enables the synchronization process to simultaneously consider the outdated yet more generalized global model and the up-to-date yet potentially overfitted local model. Particularly in circumstances where delays are substantial, the system will benefit from preserving a portion of the local model instead of fully synchronizing it with an outdated global model. This approach ensures that the most timely insights derived from the local models are maintained.

C. Adaptive Parameter Control for DFL

Next, we analyze the behavior of DFL through parameter tuning described in Algorithm 2.

1) *Impact of delay on the choice of α* : We explore the effect of various values of delay on the selection of the combiner weight α . The delay is increased incrementally from $\Delta = 5$ to $\Delta = 25$ in steps of 5, while $\tau_k = \tau = 30$ is kept constant. Fig. 6(a) illustrates the average value of α generated by Algorithm 2 across global synchronizations. It is evident from the figure that α increases as the delay increases for both CNN and SVM. This aligns with the intuition that as the delay increases, DFL would place more emphasis on the local model at the instance of local

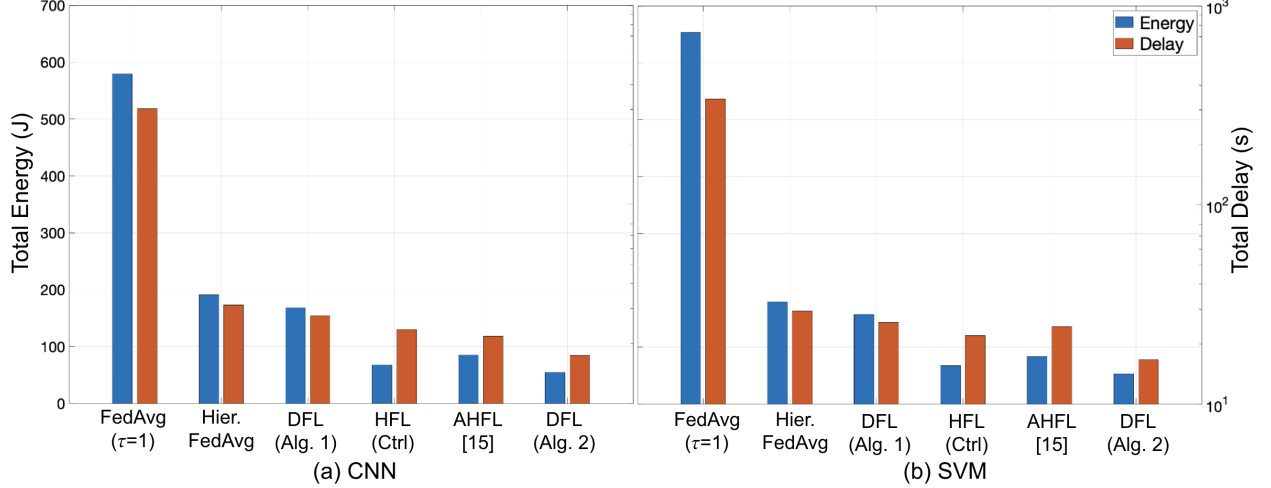


FIGURE 7: Comparison of DFL with adaptive parameter control (Algorithm 2) to the baselines in terms of total energy and delay incurred to reach 80% testing accuracy. We see that DFL obtains substantial improvements in both metrics for both CNN and SVM models.

model synchronization with the global model since the global model becomes more obsolete as the delay increases. Furthermore, as delay reaches a threshold, the selection of α ceases to increase due to the constraint in (\mathcal{P}) , limiting it to a feasible range. Algorithm 2's ability to ensure feasible α values is vital for the convergence behavior of DFL described in Theorem 1.

2) *Impact of data diversity on the choice of α* : We explore the impact of levels of data diversity across edge devices on the choice of combiner weight α obtained under Algorithm 2. We increase the data diversity by reducing the number of labels in each device's local dataset. We consider $\Delta = 10$ and $\tau_k = \tau = 30$. Fig. 6(b) indicates that α decreases as data diversity increases for both CNN and SVM. This is because local models diverge more from each other when data diversity is high, making the global model's contribution more critical (i.e., reduction in α) in aligning the local models of the devices.

3) *Enhanced resource efficiency in comparison to baseline methods*: The results presented in Fig. 7 compare the performance of DFL with adaptive parameter control (Algorithm 2) with five baseline approaches: (i) FL with full device participation and $\tau = 1$; (ii) hierarchical FL with $\alpha = 0$, $\tau = 20$, where local aggregations are performed after every 5 local model updates; (iii) DFL with fixed parameters (Algorithm 1) with $\alpha = 0.5$, $\tau = 20$, where local aggregations are performed after every 5 local model updates; (iv) HFL with parameter control, constructed by setting $\alpha = 0$ in the DFL control algorithm, thereby reducing the DFL's global aggregation to the standard global aggregation method in [12]–[17] and (v) Adaptive Hierarchical Federated Learning

(AHFL), which incorporates an adaptive control framework to efficiently manage resources [15]. Two metrics are used to compare the performance: (M_1) total energy consumption and (M_2) total delay, each measured upon reaching 80% testing accuracy. For (M_1), the results indicated by the blue bars of Fig. 7(a) & (b) show that DFL with adaptive parameter control significantly outperforms baseline approaches. Specifically, DFL requires 91.8% and 90.5% less energy than baseline (i), 71.4% and 70.4% less energy than baseline (ii), 67.5% and 66.1% less energy than baseline (iii), 19.9% and 21.1% less energy than baseline (iv), and 35.7% and 36.3% less energy than baseline (v) for CNN and SVM models, respectively. Similarly, for (M_2), DFL requires substantially less communication delay than both baseline approaches as shown in the red bars of Fig. 7(a) & (b). Specifically, DFL requires 94.2% and 95.1% less delay than baseline (i), 44.1% and 43.2% less delay than baseline (ii), 36.6% and 35.1% less delay than baseline (iii) 25.8% and 24.5% less delay than baseline (iv), and 20% and 22.5% less delay than baseline (v) for CNN and SVM models, respectively. These results demonstrate the improvements in resource-efficiency provided by DFL with adaptive parameter control, attributed to its parameter tuning approach that concurrently considers the tradeoff between the optimality gap, as derived in Theorem 1, the communication delay, and the energy consumption. The improvement of 20 – 25% over baseline (iv) in both metrics in particular highlights the benefit provided by our local-global model combiner strategy.

VI. CONCLUSION AND FUTURE WORK

In this work, we proposed DFL, which is a novel methodology that aims to improve the efficiency of distributed machine learning model training by mitigating the round-trip communication delay between the edge and the cloud. DFL quantifies the effects of delay and modifies the FL algorithm by introducing a linear local-global model combiner used in the local model synchronization steps. We investigated the convergence behavior of DFL under a generalized data heterogeneity metric and obtained a set of conditions to achieve sub-linear convergence. Based on these characteristics, we developed an adaptive control algorithm that adjusts the learning rate, local aggregation rounds, combiner weight, and global synchronization periods. Our numerical evaluation showed that DFL leads to a faster global model convergence, lower resource consumption, and a higher robustness against communication delay compared to existing FL algorithms. Future research directions include improving the robustness of DFL against different types of network impairments, such as jitter and packet loss, and investigating its performance under flexible device participation.

REFERENCES

- [1] F. P.-C. Lin, C. G. Brinton, and N. Michelusi, "Federated learning with communication delay in edge networks," in *Proc. IEEE Int. Glob. Commun. Conf.*, 2020, pp. 1–6.
- [2] B. Wu, F. Iandola, P. H. Jin, and K. Keutzer, "Squeezedet: Unified, small, low power fully convolutional neural networks for real-time object detection for autonomous driving," in *Proc. IEEE Conf. Comput. Vision Pattern Recog. Workshops*, 2017, pp. 129–137.
- [3] M. I. Jordan and T. M. Mitchell, "Machine learning: Trends, perspectives, and prospects," *Science*, vol. 349, no. 6245, pp. 255–260, 2015.
- [4] Y. Goldberg, "Neural network methods for natural language processing," *Synthesis Lectures on Human Language Technologies*, vol. 10, no. 1, pp. 1–309, 2017.
- [5] V. Cisco, "Cisco visual networking index: Forecast and trends, 2017–2022," *White Paper*, vol. 1, 2018.
- [6] M. Chiang and T. Zhang, "Fog and iot: An overview of research opportunities," *IEEE Internet Thing J.*, vol. 3, no. 6, pp. 854–864, 2016.
- [7] A. Hard *et al.*, "Federated learning for mobile keyboard prediction," *arXiv:1811.03604*, 2018.
- [8] S. Hosseinalipour, C. G. Brinton, V. Aggarwal, H. Dai, and M. Chiang, "From federated to fog learning: Distributed machine learning over heterogeneous wireless networks," *IEEE Commun. Mag.*, vol. 58, no. 12, pp. 41–47, 2020.
- [9] J. Park, S. Samarakoon, M. Bennis, and M. Debbah, "Wireless network intelligence at the edge," *Proceedings of the IEEE*, vol. 107, no. 11, pp. 2204–2239, 2019.
- [10] H. B. McMahan, E. Moore, D. Ramage, S. Hampson, and B. A. y Arcas, "Communication-Efficient Learning of Deep Networks from Decentralized Data," in *Proc. Int. Conf. Artificial Intell. Stat.*, 2017.
- [11] W. Y. B. Lim, N. C. Luong, D. T. Hoang, Y. Jiao, Y.-C. Liang, Q. Yang, D. Niyato, and C. Miao, "Federated learning in mobile edge networks: A comprehensive survey," *IEEE Commun. Surveys & Tuts.*, 2020.
- [12] Z. Wang, H. Xu, J. Liu, H. Huang, C. Qiao, and Y. Zhao, "Resource-efficient federated learning with hierarchical aggregation in edge computing," in *Proc. IEEE Int. Conf. Comput. Commun.*, 2021, pp. 1–10.
- [13] C. Feng, H. H. Yang, D. Hu, Z. Zhao, T. Q. S. Quek, and G. Min, "Mobility-aware cluster federated learning in hierarchical wireless networks," *IEEE Trans. Wireless Commun.*, pp. 1–1, 2022.
- [14] W. Y. B. Lim, J. S. Ng, Z. Xiong, D. Niyato, C. Miao, and D. I. Kim, "Dynamic edge association and resource allocation in self-organizing hierarchical federated learning networks," *IEEE J. Sel. Areas Commun.*, vol. 39, no. 12, pp. 3640–3653, 2021.
- [15] B. Xu, W. Xia, W. Wen, P. Liu, H. Zhao, and H. Zhu, "Adaptive hierarchical federated learning over wireless networks," *IEEE Trans. Veh. Technol.*, vol. 71, no. 2, pp. 2070–2083, 2022.
- [16] S. Luo, X. Chen, Q. Wu, Z. Zhou, and S. Yu, "Hfel: Joint edge association and resource allocation for cost-efficient hierarchical federated edge learning," *IEEE Trans. Wireless Commun.*, vol. 19, no. 10, pp. 6535–6548, 2020.
- [17] N. Mhaisen, A. A. Abdellatif, A. Mohamed, A. Erbad, and M. Guizani, "Optimal user-edge assignment in hierarchical federated learning based on statistical properties and network topology constraints," *IEEE Trans. Netw. Sci. Eng.*, vol. 9, no. 1, pp. 55–66, 2022.
- [18] P. Kairouz *et al.*, "Advances and open problems in federated learning," *Foundations and Trends® in Machine Learning*, vol. 14, no. 1–2, pp. 1–210, 2021.
- [19] S. Wang *et al.*, "Adaptive federated learning in resource constrained edge computing systems," *IEEE J. Select. Areas Commun.*, vol. 37, no. 6, pp. 1205–1221, 2019.

- [20] W. Sun, S. Lei, L. Wang, Z. Liu, and Y. Zhang, "Adaptive federated learning and digital twin for industrial internet of things," *IEEE Trans. Ind. Informat.*, vol. 17, no. 8, pp. 5605–5614, 2021.
- [21] Y. Tu, Y. Ruan, S. Wagle, C. Brinton, and C. Joe-Wong, "Network-aware optimization of distributed learning for fog computing," in *Proc. IEEE Int. Conf. Comput. Commun.*, 2020.
- [22] S. Wang, M. Lee, S. Hosseinalipour, R. Morabito, M. Chiang, and C. G. Brinton, "Device sampling for heterogeneous federated learning: Theory, algorithms, and implementation," in *IEEE Conf. Comput. Commun.*, 2021, pp. 1–10.
- [23] N. H. Tran, W. Bao, A. Zomaya, M. N. H. Nguyen, and C. S. Hong, "Federated learning over wireless networks: Optimization model design and analysis," in *IEEE Int. Conf. on Comput. Commun.*, 2019, pp. 1387–1395.
- [24] M. Chen, Z. Yang, W. Saad, C. Yin, H. V. Poor, and S. Cui, "A joint learning and communications framework for federated learning over wireless networks," *IEEE Trans. Wireless Commun.*, vol. 20, no. 1, pp. 269–283, 2020.
- [25] Z. Yang, M. Chen, W. Saad, C. S. Hong, and M. Shikh-Bahaei, "Energy efficient federated learning over wireless communication networks," *IEEE Transactions on Wireless Communications*, vol. 20, no. 3, pp. 1935–1949, 2020.
- [26] F. P.-C. Lin, S. Hosseinalipour, S. S. Azam, C. G. Brinton, and N. Michelusi, "Semi-decentralized federated learning with cooperative D2D local model aggregations," *IEEE J. Sel. Areas Commun.*, 2021.
- [27] S. Hosseinalipour *et al.*, "Parallel successive learning for dynamic distributed model training over heterogeneous wireless networks," *IEEE/ACM Trans. Netw.*, 2022.
- [28] W. Shi, S. Zhou, Z. Niu, M. Jiang, and L. Geng, "Joint device scheduling and resource allocation for latency constrained wireless federated learning," *IEEE Trans. Wireless Commun.*, vol. 20, no. 1, pp. 453–467, 2021.
- [29] S. Samarakoon, M. Bennis, W. Saad, and M. Debbah, "Distributed federated learning for ultra-reliable low-latency vehicular communications," *IEEE Trans. on Commun.*, vol. 68, no. 2, pp. 1146–1159, 2020.
- [30] Z. Zhao, J. Xia, L. Fan, X. Lei, G. K. Karagiannidis, and A. Nallanathan, "System optimization of federated learning networks with a constrained latency," *IEEE Trans. Veh. Technol.*, vol. 71, no. 1, pp. 1095–1100, 2022.
- [31] W. Gao, Z. Zhao, G. Min, Q. Ni, and Y. Jiang, "Resource allocation for latency-aware federated learning in industrial internet of things," *IEEE Trans. Ind. Informat.*, vol. 17, no. 12, pp. 8505–8513, 2021.
- [32] L. Liu, J. Zhang, S. Song, and K. B. Letaief, "Client-edge-cloud hierarchical federated learning," in *Proc. IEEE Int. Conf. Commun.*, 2020, pp. 1–6.
- [33] W. Y. B. Lim *et al.*, "Decentralized edge intelligence: A dynamic resource allocation framework for hierarchical federated learning," *IEEE Trans. Parallel Distrib. Syst.*, vol. 33, no. 3, pp. 536–550, 2022.
- [34] Z. Zhao, C. Feng, H. H. Yang, and X. Luo, "Federated-learning-enabled intelligent fog radio access networks: Fundamental theory, key techniques, and future trends," *IEEE Wireless Commun.*, vol. 27, no. 2, pp. 22–28, 2020.
- [35] F. Haddadpour and M. Mahdavi, "On the convergence of local descent methods in federated learning," *arXiv:1910.14425*, 2019.
- [36] M. P. Friedlander and M. Schmidt, "Hybrid deterministic-stochastic methods for data fitting," *SIAM J. Sci. Comput.*, vol. 34, no. 3, pp. A1380–A1405, 2012.
- [37] Y. Lin, S. Han, H. Mao, Y. Wang, and B. Dally, "Deep gradient compression: Reducing the communication bandwidth for distributed training," in *Proc. Int. Conf. Learn. Representations*, 2018.
- [38] H. Jiang and C. Dovrolis, "Passive estimation of tcp round-trip times," *SIGCOMM Comput. Commun. Rev.*, vol. 32, no. 3, p. 75–88, jul 2002.
- [39] N. Michelusi, "Non-coherent over-the-air decentralized stochastic gradient descent," *arXiv:2211.10777*, 2022.
- [40] X. Li, K. Huang, W. Yang, S. Wang, and Z. Zhang, "On the convergence of fedavg on non-iid data," in *Proc. Conf. Learn. Representations*, 2020.
- [41] D. Tse and P. Viswanath, *Fundamentals of wireless communication*. Cambridge university press, 2005.

- [42] S. Hosseinalipour *et al.*, “Multi-stage hybrid federated learning over large-scale D2D-enabled fog networks,” *IEEE/ACM Trans. Netw.*, vol. 30, no. 4, pp. 1569–1584, 2022.
- [43] Y. Nesterov, *Introductory Lectures on Convex Optimization: A Basic Course*, 1st ed. Springer Publishing Company, Incorporated, 2014.

INTRODUCTION TO NOTATIONS AND PRELIMINARIES USED IN THE PROOFS

The subnet noise-free variable before global synchronization is introduced as follows:

$$\bar{\mathbf{v}}_c^{(t+1)} = \bar{\mathbf{v}}_c^{(t)} - \eta_k \nabla \bar{F}_c(\bar{\mathbf{v}}_c^{(t)}), \quad \forall t \in \mathcal{T}_k \setminus \{t_k\}, \quad (43)$$

with the subnet noise-free variable at global synchronization is defined as

$$\bar{\mathbf{v}}_c^{(t_{k+1})} = (1 - \alpha) \bar{\mathbf{v}}_c^{(t_{k+1} - \Delta)} + \alpha \tilde{\mathbf{v}}_c^{(t_{k+1})}, \quad (44)$$

where $\tilde{\mathbf{v}}_c^{(t_{k+1})}$ is the noise-free variable right before global synchronization, as opposed to $\mathbf{v}_c^{(t_{k+1})}$ defined right after global synchronization. Similarly, the global noise-free variable is defined as

$$\bar{\mathbf{v}}^{(t+1)} = \sum_{d=1}^N \varrho_d \bar{\mathbf{v}}_d^{(t+1)} \quad \forall t \in \mathcal{T}_k. \quad (45)$$

The following noise terms used in the appendices are defined as follows:

$$e_1^{(t)} \triangleq \left(\mathbb{E} \left[\sum_{c=1}^N \varrho_c \sum_{j \in \mathcal{S}_c} \rho_{j,c} \|\mathbf{w}_i^{(t)} - \bar{\mathbf{v}}_c^{(t)}\|^2 \right] \right)^{1/2}, \quad (46)$$

$$e_2^{(t)} \triangleq \sum_{c=1}^N \varrho_c \|\bar{\mathbf{v}}_c^{(t)} - \bar{\mathbf{v}}^{(t)}\|, \quad (47)$$

$$e_3^{(t)} \triangleq \|\bar{\mathbf{v}}^{(t)} - \mathbf{w}^*\|. \quad (48)$$

APPENDIX A

PROOF OF THEOREM 1

Theorem 1. *Under Assumptions 1, 2 and 3, if $\eta_k = \frac{\eta_{\max}}{1+\gamma k}$, $\forall k$ and $|\mathcal{T}_k| \leq \tau$, $\forall k$, using DFL for ML model training, the distance between the global model and the optimum at global synchronization can be bounded as*

$$\mathbb{E}[\|\bar{\mathbf{w}}^{(t_k)} - \mathbf{w}^*\|^2] \leq 2Y_1^2 \eta_k + 2Y_3^2 \eta_k^2, \quad (49)$$

where $\eta_{\max} < \min \left\{ \frac{2}{\beta + \mu}, \frac{(\tau - \Delta)\mu}{\beta^2[(1 + \lambda_+)^{\tau - 1 - \tau\lambda_+}]} \right\}$, $\gamma < \min \{1 - (1 - \mu\eta_{\max})^{2(\tau - \Delta)}, C_3\eta_{\max}\beta\}$,

$$\alpha < \alpha^* \triangleq \frac{1}{\frac{C_2\eta_{\max}^2}{\eta_{\max}\beta C_3 - \gamma} 2\omega C_2(1 + \gamma) + (1 + \gamma)(1 + \lambda_+)^{\tau}}, \quad (50)$$

$$Y_1 \triangleq \sqrt{\frac{(\tau - (1 - \alpha)\Delta)(\sigma^2 + \phi^2)\eta_{\max}}{C_1 - \gamma}}, \quad (51)$$

$$Y_2 \triangleq \max \left\{ \frac{\eta_{\max}^2 \alpha 2\omega C_2 (1+\gamma) e_3^{(0)} + \alpha K_1 \delta (1+\gamma)}{1 - \alpha(1+\gamma)(1+\lambda_+)^{\tau}}, \frac{\frac{K_1 \delta}{\eta_{\max} 2\omega C_2} + \frac{K_2 \delta}{\beta C_3 - \gamma}}{\frac{[1-\alpha(1+\gamma)(1+\lambda_+)^{\tau}]}{\eta_{\max} \alpha 2\omega C_2 (1+\gamma)} - \frac{C_2}{\beta C_3 - \gamma}} \right\}, \quad (52)$$

$$Y_3 \triangleq \max \left\{ \eta_{\max} e_3^{(0)}, \frac{[C_2 Y_2 + K_2 \delta] \eta_{\max}}{\eta_{\max} \beta C_3 - \gamma} \right\}. \quad (53)$$

with $K_1 = \frac{\mu}{-\beta\lambda_+\lambda_-}[(1+\lambda_+)^{\tau} - 1]$, $K_2 = \frac{\beta}{\sqrt{1+8\omega}} \sum_{\ell=0}^{\tau-2} \binom{\tau}{\ell+2} [\lambda_+^{\ell+1} - \lambda_-^{\ell+1}]$, $C_1 = 1 - ((1 - \alpha)(1 - \mu\eta_{\max})^{2(\tau-\Delta)} + \alpha(1 - \mu\eta_{\max})^{2\tau})$, $C_2 = \frac{2\beta}{\sqrt{8\omega+1}}[(1+\lambda_+)^{\tau} - 1]$, $C_3 = (\tau - \Delta)\mu/\beta - \eta_{\max}\beta[(1+\lambda_+)^{\tau} - 1 - \tau\lambda_+]$ and $\lambda_{\pm} = \frac{1}{2} - \frac{\mu}{\beta} \pm \frac{\sqrt{8\omega+1}}{2}$.

Proof. Note that

$$\sqrt{\mathbb{E}[\|\bar{\mathbf{w}}^{(t_k)} - \mathbf{w}^*\|^2]} = \sqrt{\mathbb{E}[\|\bar{\mathbf{w}}^{(t_k)} - \bar{\mathbf{v}}^{(t_k)} + \bar{\mathbf{v}}^{(t_k)} - \mathbf{w}^*\|^2]} \quad (54)$$

$$\leq \sqrt{\mathbb{E}[\|\bar{\mathbf{w}}^{(t_k)} - \bar{\mathbf{v}}^{(t_k)}\|^2]} + \|\bar{\mathbf{v}}^{(t_k)} - \mathbf{w}^*\| \quad (55)$$

$$= \sqrt{\mathbb{E}[\|\sum_{c=1}^N \varrho_c \sum_{j \in \mathcal{S}_c} \rho_{j,c} (\mathbf{w}_j^{(t_k)} - \bar{\mathbf{v}}_c^{(t_k)})\|^2]} + \|\bar{\mathbf{v}}^{(t_k)} - \mathbf{w}^*\| \quad (56)$$

$$\leq \sqrt{\sum_{c=1}^N \varrho_c \sum_{j \in \mathcal{S}_c} \rho_{j,c} \mathbb{E}[\|\mathbf{w}_j^{(t_k)} - \bar{\mathbf{v}}_c^{(t_k)}\|^2]} + \|\bar{\mathbf{v}}^{(t_k)} - \mathbf{w}^*\| = e_1^{(t_k)} + e_3^{(t_k)}, \quad (57)$$

and therefore

$$\mathbb{E}[\|\bar{\mathbf{w}}^{(t_k)} - \mathbf{w}^*\|^2] \leq (e_1^{(t_k)} + e_3^{(t_k)})^2 \leq 2(e_1^{(t_k)})^2 + 2(e_3^{(t_k)})^2. \quad (58)$$

We now show by induction that $e_1^{(t_k)} \leq Y_1 \sqrt{\eta_k}$, $e_2^{(t_k)} \leq Y_2 \eta_k$ and $e_3^{(t_k)} \leq Y_3 \eta_k$ with Y_1 , Y_2 and Y_3 defined in (51), (52) and (53). The conditions trivially holds at the beginning of training at $k = 0$ since $Y_1 \geq 0$, $Y_2 \geq 0$ and $Y_3 \geq \eta_{\max} e_3^{(0)}$. Now, assume $e_1^{(t_k)} \leq Y_1 \sqrt{\eta_k}$, $e_2^{(t_k)} \leq Y_2 \eta_k$ and $e_3^{(t_k)} \leq Y_3 \eta_k$ for a certain $k \geq 0$. We prove the condition holds for $k + 1$ as well.

To show $e_1^{(t_{k+1})} \leq \sqrt{\eta_{k+1}} Y_1$, we use (72) of Proposition 1 and the induction hypothesis ($e_1^{(t_k)} \leq \sqrt{\eta_k} Y_1$), yielding the sufficient condition

$$(1 - \eta_k / \eta_{\max} C_1) \eta_k Y_1^2 + \eta_k^2 (\tau - (1 - \alpha) \Delta) (\sigma^2 + \phi^2) - \eta_{k+1} Y_1^2 \leq 0. \quad (59)$$

Using the expression of $\eta_k = \frac{\eta_{\max}}{1+\gamma k}$, the above condition is equivalent to

$$-[C_1 - \gamma] Y_1^2 + \eta_{\max} (\tau - (1 - \alpha) \Delta) (\sigma^2 + \phi^2) - \gamma Y_1^2 \frac{\gamma}{1 + \gamma(k+1)} \leq 0.$$

To satisfy the condition for all $k \geq 0$, the above condition is equivalent to

$$\eta_{\max} (\tau - (1 - \alpha) \Delta) (\sigma^2 + \phi^2) \leq [C_1 - \gamma] Y_1^2,$$

which is indeed verified since $\gamma < 1 - (1 - \mu\eta_{\max})^{2(\tau-\Delta)} \leq C_1$ and $Y_1^2 = \frac{(\tau-(1-\alpha)\Delta)(\sigma^2+\phi^2)\eta_{\max}}{C_1-\gamma}$.

This completes the induction for $e_1^{(t_k)}$, showing that $(e_1^{(t_k)})^2 \leq \eta_k Y_1^2$, $\forall k$.

To show $e_2^{(t_{k+1})} \leq \eta_{k+1} Y_2$, we use (73) of Proposition 1 and the induction hypothesis ($e_2^{(t_k)} \leq \eta_k Y_2$), yielding the sufficient condition

$$\alpha(1 + \lambda_+)^{\tau} \eta_k Y_2 + \alpha 2\omega C_2 \eta_k^2 Y_3 + \alpha K_1 \eta_k \delta - \eta_{k+1} Y_2 \leq 0, \quad (60)$$

Using the expression of $\eta_k = \frac{\eta_{\max}}{1+\gamma k}$, the above condition can be written as:

$$\frac{\alpha(1 + \lambda_+)^{\tau} Y_2}{\eta_{\max}} + \alpha 2\omega C_2 Y_3 + \frac{\alpha K_1 \delta}{\eta_{\max}} - \frac{Y_2}{\eta_{\max}(1 + \gamma)} - \frac{Y_2 \gamma^2 k}{\eta_{\max}(1 + \gamma(k + 1))(1 + \gamma)} - \frac{\alpha 2\omega C_2 Y_3 \gamma k}{1 + \gamma k} \leq 0, \quad (61)$$

To satisfy the condition for all $k \geq 0$, the above condition is equivalent to

$$\frac{[1 - \alpha(1 + \gamma)(1 + \lambda_+)^{\tau}] Y_2 - \alpha K_1 \delta (1 + \gamma)}{\eta_{\max}} - \alpha 2\omega C_2 Y_3 (1 + \gamma) \geq 0. \quad (62)$$

To show $e_3^{(t_{k+1})} \leq \eta_{k+1} Y_3$, we use (74) of Proposition 1 and the induction hypothesis ($e_3^{(t_k)} \leq \eta_k Y_3$), yielding the sufficient condition

$$(1 - \eta_k \beta C_3) Y_3 \eta_k + [C_2 Y_2 + K_2 \delta] \eta_k^2 - Y_3 \eta_{k+1} \leq 0. \quad (63)$$

Using the expression of $\eta_k = \frac{\eta_{\max}}{1+\gamma k}$, the above condition can be written as:

$$Y_3 [\gamma - \eta_{\max} \beta C_3] + [C_2 Y_2 + K_2 \delta] \eta_{\max} - Y_3 \gamma^2 (1 + \gamma k + \gamma) \leq 0. \quad (64)$$

To satisfy the condition for all $k \geq 0$, the above condition is equivalent to

$$Y_3 [\gamma - \eta_{\max} \beta C_3] + [C_2 Y_2 + K_2 \delta] \eta_{\max} \leq 0. \quad (65)$$

To show $e_2^{(t_k)} \leq \eta_{k+1} Y_2$ and $e_3^{(t_k)} \leq \eta_{k+1} Y_3$, the conditions $e_3^{(t_k)} \geq \eta_{\max} e_3^{(0)}$, (62) and (65) need to be satisfied simultaneously. To satisfy this, we need $\gamma < C_3 \eta_{\max} \beta$ and

$$Y_3 \geq \eta_{\max} e_3^{(0)}, \quad (66)$$

$$Y_3 \leq \frac{[1 - \alpha(1 + \gamma)(1 + \lambda_+)^{\tau}] Y_2 - \alpha K_1 \delta (1 + \gamma)}{\eta_{\max} \alpha 2\omega C_2 (1 + \gamma)}, \quad (67)$$

and

$$Y_3 \geq \frac{[C_2 Y_2 + K_2 \delta] \eta_{\max}}{\eta_{\max} \beta C_3 - \gamma}. \quad (68)$$

Using the definition of Y_3 in (53), the conditions above become equivalent to

$$Y_3 \leq \frac{[1 - \alpha(1 + \gamma)(1 + \lambda_+)^{\tau}] Y_2 - \alpha K_1 \delta (1 + \gamma)}{\eta_{\max} \alpha 2\omega C_2 (1 + \gamma)}, \quad (69)$$

yielding the sufficient conditions

$$\eta_{\max} e_3^{(0)} \leq \frac{[1 - \alpha(1 + \gamma)(1 + \lambda_+)^{\tau}]Y_2 - \alpha K_1 \delta(1 + \gamma)}{\eta_{\max} \alpha 2\omega C_2(1 + \gamma)}, \quad (70)$$

and

$$\frac{[C_2 Y_2 + K_2 \delta] \eta_{\max}}{\eta_{\max} \beta C_3 - \gamma} \leq \frac{[1 - \alpha(1 + \gamma)(1 + \lambda_+)^{\tau}]Y_2 - \alpha K_1 \delta(1 + \gamma)}{\eta_{\max} \alpha 2\omega C_2(1 + \gamma)}, \quad (71)$$

which can be verified since $\alpha < \alpha^*$ together with the definition of Y_2 given in (52). This completes the induction showing that $e_2^{(t_k)} \leq \eta_{k+1} Y_2$ and $e_3^{(t_k)} \leq \eta_{k+1} Y_3$. Finally, applying the result of induction for $e_1^{(t_k)}$, $e_2^{(t_k)}$ and $e_3^{(t_k)}$ into (58) completes the proof. \square

APPENDIX B

PROOF OF PROPOSITION 1

Proposition 1. *Under Assumptions 1, 2 and 3, if $\eta_k = \frac{\eta_{\max}}{1+\gamma_k}$, where $\eta_{\max} < \min \left\{ \frac{2}{\beta+\mu}, \frac{(\tau-\Delta)\mu}{\beta^2[(1+\lambda_+)^{\tau-1}-\tau\lambda_+]} \right\}$, using DFL for ML model training, $(e_1^{(t_{k+1})})^2$, $e_2^{(t_{k+1})}$ and $e_3^{(t_{k+1})}$ across global synchronizations can be bounded as*

$$(e_1^{(t_{k+1})})^2 \leq (1 - \eta_k/\eta_{\max}C_1)(e_1^{(t_k)})^2 + \eta_k^2(\tau - (1 - \alpha)\Delta)(\sigma^2 + \phi^2), \quad (72)$$

$$e_2^{(t_{k+1})} \leq \alpha(1 + \lambda_+)^{\tau} e_2^{(t_k)} + \eta_k \alpha 2\omega C_2 e_3^{(t_k)} + \eta_k \alpha K_1 \delta, \quad (73)$$

$$e_3^{(t_{k+1})} \leq (1 - \eta_k \beta C_3) e_3^{(t_k)} + C_2 \eta_k e_2^{(t_k)} + \eta_k^2 K_2 \delta, \quad (74)$$

where

$$C_1 \triangleq 1 - ((1 - \alpha)(1 - \mu\eta_{\max})^{2(\tau-\Delta)} + \alpha(1 - \mu\eta_{\max})^{2\tau}), \quad (75)$$

$$C_2 \triangleq \frac{2\beta}{\sqrt{8\omega+1}}[(1 + \lambda_+)^{\tau} - 1], \quad (76)$$

$$C_3 \triangleq (\tau - \Delta)\mu/\beta - \eta_{\max}\beta[(1 + \lambda_+)^{\tau} - 1 - \tau\lambda_+], \quad (77)$$

$$K_1 \triangleq \frac{\mu}{-\beta\lambda_+\lambda_-}[(1 + \lambda_+)^{\tau} - 1], \quad (78)$$

$$K_2 \triangleq \frac{\beta}{\sqrt{1+8\omega}} \sum_{\ell=0}^{\tau-2} \binom{\tau}{\ell+2} [\lambda_+^{\ell+1} - \lambda_-^{\ell+1}], \quad (79)$$

with λ_{\pm} defined in (107) of Lemma 2.

Proof. We prove this result by further upper bounding $e_1^{(t_{k+1})}$ in Lemma 2. Therein, we found that

$$(e_1^{(t_{k+1})})^2 \leq [(1 - \alpha)(1 - \mu\eta_k)^{2(\tau-\Delta)} + \alpha(1 - \mu\eta_k)^{2\tau}](e_1^{(t_k)})^2 + \eta_k^2(\tau - (1 - \alpha)\Delta)(\sigma^2 + \phi^2). \quad (80)$$

To bound $(e_1^{(t_{k+1})})^2$ in (80), we use the fact that $[(1 - \alpha)(1 - \mu\eta_k)^{2(\tau-\Delta)} + \alpha(1 - \mu\eta_k)^{2\tau}]$ is a convex function of $\eta_k \in [0, \eta_{\max}]$ (in fact, $\mu\eta_{\max} \leq 1$ since $\eta_{\max} \leq \frac{2}{\beta+\mu}$), hence

$$(1 - \alpha)(1 - \mu\eta_k)^{2(\tau-\Delta)} + \alpha(1 - \mu\eta_k)^{2\tau} \leq 1 - \eta_k/\eta_{\max}C_1. \quad (81)$$

Applying the result from (81) into (80), gives us the result in (72). Similarly for $e_2^{(t_{k+1})}$, we found

$$e_2^{(t_{k+1})} \leq \alpha \Pi_{+,t_{k+1}} e_2^{(t_k)} + \alpha \frac{4\omega}{\sqrt{8\omega+1}} [\Pi_{+,t_{k+1}} - 1] e_3^{(t_k)} + \alpha \frac{\mu}{-\beta^2 \lambda_+ \lambda_-} (\Pi_{+,t_{k+1}} - 1) \delta, \quad (82)$$

where $\Pi_{\{+,-\},t} = [1 + \eta_k \beta \lambda_{\{+,-\}}]^{t-t_k}$. Using convexity of $\Pi_{+,t_{k+1}}$ in $\eta_k \beta \in [0, 1]$, we bound it as $\Pi_{+,t_{k+1}} \leq 1 + \eta_k \beta [(1 + \lambda_+)^{\tau} - 1]$. Applying it into the above inequality yields

$$e_2^{(t_{k+1})} \leq \alpha (1 + \lambda_+)^{\tau} e_2^{(t_k)} + \eta_k \alpha 2\omega C_2 e_3^{(t_k)} + \eta_k \alpha K_1 \delta. \quad (83)$$

Finally, we found in (105) of Lemma 2 that

$$\begin{aligned} e_3^{(t_{k+1})} &\leq \Psi_1(\eta_k) e_3^{(t_k)} \\ &+ \underbrace{2g_3[(1 - \alpha)\Pi_{+,t_{k+1}-\Delta} + \alpha\Pi_{+,t_{k+1}} - 1]}_{(a)} e_2^{(t_k)} \\ &+ \underbrace{[(1 - \alpha)[g_5(\Pi_{+,t_{k+1}-\Delta} - 1) + g_6(\Pi_{-,t_{k+1}-\Delta} - 1)] + \alpha[g_5(\Pi_{+,t_{k+1}} - 1) + g_6(\Pi_{-,t_{k+1}} - 1)]}_{(b)} \delta / \beta, \end{aligned} \quad (84)$$

where $\Psi_1(\eta_k)$, g_3 , g_5 and g_6 is defined in (106), (126), (128) and (129) of Lemma 2. We bound $\Psi_1(\eta_k)$ as follows. Applying the binomial expansion, we have

$$\begin{aligned} &\frac{g_1 \Pi_{+,t_k+\ell} + g_2 \Pi_{-,t_k+\ell} - 1}{\eta_k \beta} \\ &= -\ell \mu / \beta + \eta_k \beta \sum_{r=2}^{\ell} \frac{\ell!}{r!(\ell-r)!} (\eta_k \beta)^{r-2} \left[\frac{1}{2} \left(1 - \frac{1}{\sqrt{8\omega+1}}\right) \lambda_+^r + \frac{1}{2} \left(1 + \frac{1}{\sqrt{8\omega+1}}\right) \lambda_-^r \right]. \end{aligned} \quad (85)$$

Since $\lambda_- \leq \lambda_+$, $\eta_k \leq \eta_{\max}$ and $\eta_k \beta \leq 1$, we can further upper bound (85) with

$$\begin{aligned} &\frac{g_1 \Pi_{+,t_k+\ell} + g_2 \Pi_{-,t_k+\ell} - 1}{\eta_k \beta} \leq -\ell \mu / \beta + \eta_k \beta \sum_{r=2}^{\ell} \frac{\ell!}{r!(\ell-r)!} (\eta_k \beta)^{r-2} \lambda_+^r \\ &\leq -\ell \mu / \beta + \eta_{\max} \beta \sum_{r=2}^{\ell} \frac{\ell!}{r!(\ell-r)!} \lambda_+^r \\ &\stackrel{(a)}{=} -\ell \mu / \beta + \eta_{\max} \beta [(1 + \lambda_+)^{\ell} - 1 - \ell \lambda_+], \end{aligned} \quad (86)$$

where (a) comes from applying the binomial theorem. Note that $(1 + \lambda_+)^{\ell} - 1 - \ell \lambda_+ \geq 0$, $\forall \ell \geq 0$.

Combining this result into (106) of Lemma 2, it follows that

$$\begin{aligned} &\frac{\Psi_1(\eta_k) - 1}{\eta_k \beta} \leq -(\tau - (1 - \alpha)\Delta) \mu / \beta \\ &+ \eta_{\max} \beta [(1 - \alpha)(1 + \lambda_+)^{\tau-\Delta} + \alpha(1 + \lambda_+)^{\tau} - 1 - (\tau - (1 - \alpha)\Delta) \lambda_+] \end{aligned}$$

$$\leq -(\tau - \Delta)\mu/\beta + \eta_{\max}\beta[(1 + \lambda_+)^{\tau} - 1 - \tau\lambda_+] \triangleq -C_3, \quad (87)$$

where in the last inequality comes from $\tau - (1 - \alpha)\Delta \geq \tau - \Delta$ and $(1 - \alpha)(1 + \lambda_+)^{\tau - \Delta} + \alpha(1 + \lambda_+)^{\tau} - 1 - (\tau - (1 - \alpha)\Delta)\lambda_+ \leq (1 + \lambda_+)^{\tau} - 1 - \tau\lambda_+$. Therefore, under $\eta_{\max} < \frac{(\tau - \Delta)\mu}{\beta^2[(1 + \lambda_+)^{\tau - 1} - \tau\lambda_+]}$, we have $C_3 > 0$ and

$$\Psi_1(\eta_k) \leq 1 - \eta_k\beta C_3 < 1. \quad (88)$$

Next, we bound (a) in (84). Convexity of $\Pi_{+,t} - 1$ with respect to $\eta_k\beta$ and $\eta_{\max}\beta \leq 1$ implies that

$$\begin{aligned} & 2g_3[(1 - \alpha)\Pi_{+,t_{k+1}-\Delta} + \alpha\Pi_{+,t_{k+1}} - 1] \\ & \leq \eta_k \frac{2\beta}{\sqrt{8\omega + 1}} [(1 - \alpha)(1 + \lambda_+)^{\tau - \Delta} + \alpha(1 + \lambda_+)^{\tau} - 1] \leq \eta_k C_2, \end{aligned} \quad (89)$$

where g_3 is defined in (126) of Lemma 2, with

$$C_2 = \frac{2\beta}{\sqrt{8\omega + 1}} [(1 + \lambda_+)^{\tau} - 1].$$

Finally, we bound (b) in (84), using the binomial expansion and the expressions of g_5 and g_6

$$g_5(\Pi_{+,t} - 1) + g_6(\Pi_{-,t} - 1) = (\eta_k\beta)^2 \frac{1}{\sqrt{1 + 8\omega}} \sum_{\ell=0}^{t-t_k-2} \binom{t-t_k}{\ell+2} (\eta_k\beta)^{\ell} [\lambda_+^{\ell+1} - \lambda_-^{\ell+1}] \leq \eta_k^2 \beta K_2.$$

Using these bounds in (84) yield the final result in (74). \square

APPENDIX C

LEMMAS AND AUXILIARY RESULTS

To improve the tractability of the proofs, we provide a set of lemmas in the following, which will be used to obtain the main results of the paper.

Lemma 1. *For $t \in \mathcal{T}_k$ before performing global synchronization, under Assumptions 1, 2 and 3, if $\eta_k \leq \frac{2}{\mu+\beta}$, $\forall k$, using DFL for ML model training, in $t \in \mathcal{T}_k$, the one-step behaviors of $(e_1^{(t+1)})^2$, $e_2^{(t+1)}$ and $e_3^{(t+1)}$ are presented as follows:*

$$(e_1^{(t+1)})^2 \leq (1 - \mu\eta_k)^2 (e_1^{(t)})^2 + \eta_k^2 (\sigma^2 + \phi^2), \quad (90)$$

$$e_2^{(t+1)} \leq (1 + \eta_k(\beta - \mu))e_2^{(t)} + 2\omega\eta_k\beta e_3^{(t)} + \eta_k\delta, \quad (91)$$

$$e_3^{(t+1)} \leq (1 - \eta_k\mu)e_3^{(t)} + \eta_k\beta e_2^{(t)}. \quad (92)$$

Proof. To bound $e_1^{(t)}$, we first use the definition of $\mathbf{w}_i^{(t+1)}$, $\forall i \in \mathcal{S}_c$ in (13) and $\mathbf{v}_c^{(t+1)}$ in (43) to get,

$$\begin{aligned} \mathbf{w}_i^{(t+1)} - \bar{\mathbf{v}}_c^{(t+1)} &= (1 - \Theta_c^{(t)})(\mathbf{w}_i^{(t)} - \eta_k \nabla F_i(\mathbf{w}_i^{(t)}) - \bar{\mathbf{v}}_c^{(t)} + \eta_k \nabla \bar{F}_c(\bar{\mathbf{v}}_c^{(t)})) \\ &+ \Theta_c^{(t)}(\bar{\mathbf{w}}_c^{(t)} - \eta_k \sum_{j \in \mathcal{S}_c} \rho_{j,c} \nabla F_j(\mathbf{w}_j^{(t)}) - \bar{\mathbf{v}}_c^{(t)} + \eta_k \nabla \bar{F}_c(\bar{\mathbf{v}}_c^{(t)})) \\ &- \eta_k(1 - \Theta_c^{(t)})\mathbf{n}_i^{(t)} - \eta_k \Theta_c^{(t)} \sum_{j \in \mathcal{S}_c} \rho_{j,c} \mathbf{n}_j^{(t)}. \end{aligned} \quad (93)$$

Then,

$$\begin{aligned} (e_1^{(t+1)})^2 &\triangleq \mathbb{E} \left[\sum_{c=1}^N \varrho_c \sum_{j \in \mathcal{S}_c} \rho_{j,c} \|\mathbf{w}_j^{(t+1)} - \bar{\mathbf{v}}_c^{(t+1)}\|^2 \right] \\ &\leq \mathbb{E} \left[\sum_{c=1}^N \varrho_c (1 - \Theta_c^{(t)}) \sum_{j \in \mathcal{S}_c} \rho_{j,c} \|\mathbf{w}_j^{(t)} - \eta_k \nabla F_j(\mathbf{w}_j^{(t)}) - \bar{\mathbf{v}}_c^{(t)} + \eta_k \nabla \bar{F}_c(\bar{\mathbf{v}}_c^{(t)})\|^2 \right] \\ &+ \mathbb{E} \left[\sum_{c=1}^N \varrho_c \Theta_c^{(t)} \|\bar{\mathbf{w}}_c^{(t)} - \eta_k \sum_{j \in \mathcal{S}_c} \rho_{j,c} \nabla F_j(\mathbf{w}_j^{(t)}) - \bar{\mathbf{v}}_c^{(t)} + \eta_k \nabla \bar{F}_c(\bar{\mathbf{v}}_c^{(t)})\|^2 \right] + \eta_k^2 \sigma^2 \\ &\leq \mathbb{E} \left[\sum_{c=1}^N \varrho_c (1 - \Theta_c^{(t)}) \sum_{j \in \mathcal{S}_c} \rho_{j,c} \|\mathbf{w}_j^{(t)} - \bar{\mathbf{v}}_c^{(t)} - \eta_k (\nabla F_j(\mathbf{w}_j^{(t)}) - \nabla \bar{F}_c(\bar{\mathbf{v}}_c^{(t)}))\|^2 \right] \\ &+ \mathbb{E} \left[\sum_{c=1}^N \varrho_c \Theta_c^{(t)} \sum_{j \in \mathcal{S}_c} \rho_{j,c} \|\mathbf{w}_j^{(t)} - \eta_k \nabla F_j(\mathbf{w}_j^{(t)}) - \bar{\mathbf{v}}_c^{(t)} + \eta_k \nabla F_j(\bar{\mathbf{v}}_c^{(t)})\|^2 \right] + \eta_k^2 \sigma^2, \end{aligned} \quad (94)$$

where the last step follows from $\sum_{j \in \mathcal{S}_c} \rho_{j,c} F_j(\bar{\mathbf{v}}_c^{(t)}) = \bar{F}_c(\bar{\mathbf{v}}_c^{(t)})$, $\sum_{j \in \mathcal{S}_c} \rho_{j,c} \mathbf{w}_j^{(t)} = \bar{\mathbf{w}}_c^{(t)}$ and convexity of $\|\cdot\|^2$. Using again the fact that $\sum_{j \in \mathcal{S}_c} \rho_{j,c} F_j(\bar{\mathbf{v}}_c^{(t)}) = \bar{F}_c(\bar{\mathbf{v}}_c^{(t)})$, we further bound

$$\begin{aligned} & \sum_{j \in \mathcal{S}_c} \rho_{j,c} \|\mathbf{w}_j^{(t)} - \bar{\mathbf{v}}_c^{(t)} - \eta_k(\nabla F_j(\mathbf{w}_j^{(t)}) - \nabla \bar{F}_c(\bar{\mathbf{v}}_c^{(t)}))\|^2 \\ &= \sum_{j \in \mathcal{S}_c} \rho_{j,c} \|\mathbf{w}_j^{(t)} - \bar{\mathbf{v}}_c^{(t)} - \eta_k(\nabla F_j(\mathbf{w}_j^{(t)}) - \nabla F_j(\bar{\mathbf{v}}_c^{(t)})) - \eta_k(\nabla F_j(\bar{\mathbf{v}}_c^{(t)}) - \nabla \bar{F}_c(\bar{\mathbf{v}}_c^{(t)}))\|^2 \\ &\leq \sum_{j \in \mathcal{S}_c} \rho_{j,c} \|\mathbf{w}_j^{(t)} - \bar{\mathbf{v}}_c^{(t)} - \eta_k(\nabla F_j(\mathbf{w}_j^{(t)}) - \eta_k \nabla F_j(\bar{\mathbf{v}}_c^{(t)}))\|^2 + \eta_k^2 \sum_{j \in \mathcal{S}_c} \rho_{j,c} \|\nabla F_j(\bar{\mathbf{v}}_c^{(t)}) - \nabla \bar{F}_c(\bar{\mathbf{v}}_c^{(t)})\|^2. \end{aligned}$$

Furthermore, $\|\nabla F_j(\bar{\mathbf{v}}_c^{(t)}) - \nabla \bar{F}_c(\bar{\mathbf{v}}_c^{(t)})\|^2 \leq (\delta_c + 2\omega_c \beta \|\bar{\mathbf{v}}_c^{(t)} - \mathbf{w}^*\|)^2 \leq 2\delta_c^2 + 4\omega_c \beta \|\bar{\mathbf{v}}_c^{(t)} - \mathbf{w}^*\|^2$ (Definition 2). Combining these bounds together into (95) and using Fact 2 yields

$$\begin{aligned} (e_1^{(t+1)})^2 &\leq (1 - \mu\eta_k)^2 \mathbb{E} \left[\sum_{c=1}^N \varrho_c \sum_{j \in \mathcal{S}_c} \rho_{j,c} \|\bar{\mathbf{w}}_j^{(t)} - \bar{\mathbf{v}}_c^{(t)}\|^2 \right] \\ &\quad + \eta_k^2 \sum_{c=1}^N \varrho_c (1 - \Theta_c^{(t)}) (2\delta_c^2 + 4\omega_c^2 \beta^2 \|\bar{\mathbf{v}}_c^{(t)} - \mathbf{w}^*\|^2) + \eta_k^2 \sigma^2. \end{aligned} \quad (95)$$

Assuming that $\Theta_c^{(t)}$ is chosen such that $\sum_{c=1}^N \varrho_c (1 - \Theta_c^{(t)}) (2\delta_c^2 + 4\omega_c^2 \beta^2 \|\bar{\mathbf{v}}_c^{(t)} - \mathbf{w}^*\|^2) \leq \phi^2$, (this will be part of the control algorithm, see Assumption 3) we can further upper bound (95) and obtain the result in (90).

Next, we bound e_2 . Using (43) we find that

$$\bar{\mathbf{v}}^{(t+1)} = \bar{\mathbf{v}}^{(t)} - \eta_k \sum_{d=1}^N \varrho_d \nabla \bar{F}_d(\bar{\mathbf{v}}_d^{(t)}). \quad (96)$$

It then follows, after algebraic manipulations,

$$\begin{aligned} \bar{\mathbf{v}}_c^{(t+1)} - \bar{\mathbf{v}}^{(t+1)} &= \bar{\mathbf{v}}_c^{(t)} - \bar{\mathbf{v}}^{(t)} - \eta_k \left(\nabla \bar{F}_c(\bar{\mathbf{v}}_c^{(t)}) - \nabla \bar{F}_c(\bar{\mathbf{v}}^{(t)}) \right) \\ &\quad + \eta_k \sum_{d=1}^N \varrho_d \left(\nabla \bar{F}_d(\bar{\mathbf{v}}_d^{(t)}) - \nabla \bar{F}_d(\bar{\mathbf{v}}^{(t)}) \right) - \eta_k \left(\nabla \bar{F}_c(\bar{\mathbf{v}}^{(t)}) - \nabla F(\bar{\mathbf{v}}^{(t)}) \right). \end{aligned} \quad (97)$$

Taking the norm-2 of both hand sides of the above equality and applying the triangle inequality results in

$$\begin{aligned} \|\bar{\mathbf{v}}_c^{(t+1)} - \bar{\mathbf{v}}^{(t+1)}\| &\leq \|\bar{\mathbf{v}}_c^{(t)} - \bar{\mathbf{v}}^{(t)} - \eta_k [\nabla \bar{F}_c(\bar{\mathbf{v}}_c^{(t)}) - \nabla \bar{F}_c(\bar{\mathbf{v}}^{(t)})]\| \\ &\quad + \eta_k \sum_{d=1}^N \varrho_d \|\nabla \bar{F}_d(\bar{\mathbf{v}}_d^{(t)}) - \nabla \bar{F}_d(\bar{\mathbf{v}}^{(t)})\| + \eta_k \|\nabla \bar{F}_c(\bar{\mathbf{v}}^{(t)}) - \nabla F(\bar{\mathbf{v}}^{(t)})\|. \end{aligned} \quad (98)$$

Using β -smoothness of $F_i(\cdot), \forall i$ (hence of $\bar{F}_d(\cdot)$), Definition 1, Fact 2, and adding over $\sum_c \rho_c$, we further bound the right hand side of (98) as

$$e_2^{(t+1)} \triangleq \sum_{c=1}^N \varrho_c \|\bar{\mathbf{v}}_c^{(t+1)} - \bar{\mathbf{v}}^{(t+1)}\| \leq (1 + \eta_k(\beta - \mu)) \sum_{c=1}^N \varrho_c \|\bar{\mathbf{v}}_c^{(t)} - \bar{\mathbf{v}}^{(t)}\| + 2\omega\eta_k\beta \|\bar{\mathbf{v}}^{(t)} - \mathbf{w}^*\| + \eta_k\delta, \quad (99)$$

which proves (90). Finally, we bound e_3 . From (96), we get

$$\bar{\mathbf{v}}^{(t+1)} - \mathbf{w}^* = \bar{\mathbf{v}}^{(t)} - \mathbf{w}^* - \eta_k \nabla F(\bar{\mathbf{v}}^{(t)}) - \eta_k \sum_{d=1}^N \varrho_d [\nabla \bar{F}_d(\bar{\mathbf{v}}_d^{(t)}) - \nabla \bar{F}_d(\bar{\mathbf{v}}^{(t)})]. \quad (100)$$

Taking the norm of both hand sides of the above equality and applying the triangle inequality gives us

$$\|\bar{\mathbf{v}}^{(t+1)} - \mathbf{w}^*\| \leq \|\bar{\mathbf{v}}^{(t)} - \mathbf{w}^* - \eta_k \nabla F(\bar{\mathbf{v}}^{(t)})\| + \eta_k \sum_{d=1}^N \varrho_d \|\nabla \bar{F}_d(\bar{\mathbf{v}}_d^{(t)}) - \nabla \bar{F}_d(\bar{\mathbf{v}}^{(t)})\|. \quad (101)$$

Using β -smoothness of $F_i(\cdot)$ (hence of $\bar{F}_d(\cdot)$) and Fact 2, we further bound

$$e_3^{(t+1)} \triangleq \|\bar{\mathbf{v}}^{(t+1)} - \mathbf{w}^*\| \leq (1 - \eta_k\mu) \|\bar{\mathbf{v}}^{(t)} - \mathbf{w}^*\| + \eta_k\beta \sum_{d=1}^N \varrho_d \|\bar{\mathbf{v}}_d^{(t)} - \bar{\mathbf{v}}^{(t)}\|, \quad (102)$$

yielding (92). \square

Lemma 2. *Under Assumptions 1, 2 and 3, if $\eta_k \leq \frac{2}{\beta+\mu}$, $\forall k$, using DFL for ML model training, $e_1^{t_{k+1}}$, $e_2^{t_{k+1}}$ and $e_3^{t_{k+1}}$ across global synchronization periods can be bounded as*

$$(e_1^{t_{k+1}})^2 \leq [(1 - \alpha)(1 - \mu\eta_k)^{2(\tau-\Delta)} + \alpha(1 - \mu\eta_k)^{2\tau}](e_1^{(t_k)})^2 + [\tau - (1 - \alpha)\Delta]\eta_k^2(\sigma^2 + \phi^2), \quad (103)$$

$$e_2^{(t_{k+1})} \leq \alpha\Pi_{+,t_{k+1}}e_2^{(t_k)} + \alpha\frac{4\omega}{\sqrt{8\omega+1}}[\Pi_{+,t_{k+1}} - 1]e_3^{(t_k)} + \alpha\frac{\mu}{-\beta^2\lambda_+\lambda_-}[\Pi_{+,t_{k+1}} - 1]\delta, \quad (104)$$

$$\begin{aligned} e_3^{(t_{k+1})} &\leq \Psi_1(\eta_k)e_3^{(t_k)} + 2g_3[(1 - \alpha)\Pi_{+,t_{k+1}-\Delta} + \alpha\Pi_{+,t_{k+1}} - 1]e_2^{(t_k)} \\ &+ [(1 - \alpha)[g_5(\Pi_{+,t_{k+1}-\Delta} - 1) + g_6(\Pi_{-,t_{k+1}-\Delta} - 1)] + \alpha[g_5(\Pi_{+,t_{k+1}} - 1) + g_6(\Pi_{-,t_{k+1}} - 1)]\delta/\beta. \end{aligned} \quad (105)$$

where

$$\Psi_1(\eta_k) \triangleq (1 - \alpha)[g_1\Pi_{+,t_{k+1}-\Delta} + g_2\Pi_{-,t_{k+1}-\Delta}] + \alpha[g_1\Pi_{+,t_{k+1}} + g_2\Pi_{-,t_{k+1}}] \quad (106)$$

and

$$\lambda_{\pm} = \frac{1}{2} - \frac{\mu}{\beta} \pm \frac{\sqrt{8\omega+1}}{2}, \quad (107)$$

with $\lambda_+ > 0$, $\lambda_- < 0$, $\Pi_{\{+,-\},t} = [1 + \eta_k\beta\lambda_{\{+,-\}}]^{t-t_k}$ and g_1, g_2, g_3, g_5, g_6 defined in (124), (125), (126), (128), (129)

Proof. A. Obtaining the upper bound of $e_1^{(t_{k+1})}$ at global synchronization

Using the one-step dynamics in (90), Lemma 1, we find before global synchronization

$$\begin{aligned} (e_1^{(t)})^2 &\leq (1 - \mu\eta_k)^{2(t-t_k)}(e_1^{(t_k)})^2 + \sum_{\ell=0}^{t-t_k-1} (1 - \mu\eta_k)^{2\ell}\eta_k^2(\sigma^2 + \phi^2) \\ &\leq (1 - \mu\eta_k)^{2(t-t_k)}(e_1^{(t_k)})^2 + (t - t_k)\eta_k^2(\sigma^2 + \phi^2). \end{aligned} \quad (108)$$

Next, we obtain the behavior of $e_1^{(t)}$ at global synchronization by using the definition of $\mathbf{w}_i^{(t)}$, $\bar{\mathbf{v}}_c^{(t)}$ and the global synchronization scheme in (16) as follows:

$$\mathbf{w}_i^{(t_{k+1})} - \bar{\mathbf{v}}_c^{(t_{k+1})} = (1 - \alpha) \sum_{d=1}^N \varrho_d \sum_{j \in \mathcal{S}_d} \rho_{j,d} (\mathbf{w}_j^{(t_{k+1}-\Delta)} - \bar{\mathbf{v}}_d^{(t_{k+1}-\Delta)}) + \alpha \left(\tilde{\mathbf{w}}_i^{(t_{k+1})} - \tilde{\mathbf{v}}_c^{(t_{k+1})} \right), \quad (109)$$

where $\tilde{\mathbf{w}}_i^{(t_{k+1})}$ and $\tilde{\mathbf{v}}_c^{(t_{k+1})}$ are the local model and subnet noise-free variables right before global synchronization, as opposed to $\mathbf{w}_i^{(t_{k+1})}$ and $\mathbf{v}_c^{(t_{k+1})}$ defined right after global synchronization. Taking the squared norm on both hand sides of the above equality and applying Jensen's inequality (convexity of $\|\cdot\|^2$) yields

$$\|\mathbf{w}_i^{(t_{k+1})} - \bar{\mathbf{v}}_c^{(t_{k+1})}\|^2 \leq (1 - \alpha) \sum_{d=1}^N \varrho_d \sum_{j \in \mathcal{S}_d} \rho_{j,d} \|\mathbf{w}_j^{(t_{k+1}-\Delta)} - \bar{\mathbf{v}}_d^{(t_{k+1}-\Delta)}\|^2 + \alpha \|\tilde{\mathbf{w}}_i^{(t_{k+1})} - \tilde{\mathbf{v}}_c^{(t_{k+1})}\|^2. \quad (110)$$

Therefore,

$$\begin{aligned} (e_1^{(t_{k+1})})^2 &= \sum_{c=1}^N \varrho_c \sum_{i \in \mathcal{S}_c} \rho_{i,c} \|\mathbf{w}_i^{(t_{k+1})} - \bar{\mathbf{v}}_c^{(t_{k+1})}\|^2 \\ &\leq (1 - \alpha) \sum_{c=1}^N \varrho_c \sum_{j \in \mathcal{S}_c} \rho_{j,c} \|\mathbf{w}_j^{(t_{k+1}-\Delta)} - \bar{\mathbf{v}}_c^{(t_{k+1}-\Delta)}\|^2 + \alpha \sum_{c=1}^N \varrho_c \sum_{j \in \mathcal{S}_c} \rho_{j,c} \left\| \tilde{\mathbf{w}}_j^{(t_{k+1})} - \tilde{\mathbf{v}}_c^{(t_{k+1})} \right\|^2. \end{aligned} \quad (111)$$

Note that the terms above are upper bounded by (108) before global synchronization, hence they can be bounded as

$$\begin{aligned} \sum_{c=1}^N \varrho_c \sum_{j \in \mathcal{S}_c} \rho_{j,c} \|\mathbf{w}_j^{(t_{k+1}-\Delta)} - \bar{\mathbf{v}}_c^{(t_{k+1}-\Delta)}\|^2 &\leq (1 - \mu\eta_k)^{2(\tau-\Delta)}(e_1^{(t_k)})^2 + [\tau - \Delta]\eta_k^2(\sigma^2 + \phi^2), \\ \sum_{c=1}^N \varrho_c \sum_{j \in \mathcal{S}_c} \rho_{j,c} \left\| \tilde{\mathbf{w}}_j^{(t_{k+1})} - \tilde{\mathbf{v}}_c^{(t_{k+1})} \right\|^2 &\leq (1 - \mu\eta_k)^{2\tau}(e_1^{(t_k)})^2 + \tau\eta_k^2(\sigma^2 + \phi^2). \end{aligned}$$

Using these bounds in (111) yields (103).

B. Solving the coupled dynamics between e_2 and e_3

Let $\mathbf{x}^{(t)} = \begin{bmatrix} e_2^{(t)} & e_3^{(t)} \end{bmatrix}^\top$, with e_2 and e_3 defined in (47) and (48). Using the one-step dynamics found in Lemma 2 for $t \in \mathcal{T}_k$, we find (here, the vector inequality is entry-wise)

$$\mathbf{x}^{(t+1)} \leq [\mathbf{I} + \eta_k \beta \mathbf{B}] \mathbf{x}^{(t)} + \eta_k \beta \mathbf{z}, \quad (112)$$

where $\mathbf{z} = \mathbf{e}_1 \delta / \beta$, $\mathbf{B} = \begin{bmatrix} 1 - \frac{\mu}{\beta} & 2\omega \\ 1 & -\frac{\mu}{\beta} \end{bmatrix}$, $\mathbf{e}_1 = [1, 0]^\top$. We also define $\mathbf{e}_2 = [0, 1]^\top$. We aim to derive an upper bound on $\mathbf{x}^{(t)}$ denoted by $\mathbf{x}^{(t)} \leq \bar{\mathbf{x}}^{(t)}$. Using the above inequality, such upper bound is given by the recursion

$$\bar{\mathbf{x}}^{(t+1)} = [\mathbf{I} + \eta_k \beta \mathbf{B}] \bar{\mathbf{x}}^{(t)} + \eta_k \beta \mathbf{z}, \quad \forall t \in \mathcal{T}_k, \quad (113)$$

initialized as $\bar{\mathbf{x}}^{(t_k)} = \mathbf{x}^{(t_k)}$. To solve the coupled dynamic, we first apply eigen-decomposition on \mathbf{B} yielding $\mathbf{B} = \mathbf{U} \mathbf{D} \mathbf{U}^{-1}$, where

$$\mathbf{D} = \begin{bmatrix} \lambda_+ & 0 \\ 0 & \lambda_- \end{bmatrix}, \quad \mathbf{U} = \begin{bmatrix} \frac{1}{2}(1 + \sqrt{8\omega + 1}) & -\frac{1}{2}(\sqrt{8\omega + 1} - 1) \\ 1 & 1 \end{bmatrix}, \quad \mathbf{U}^{-1} = \frac{1}{\sqrt{8\omega + 1}} \begin{bmatrix} 1 & \frac{1}{2}(\sqrt{8\omega + 1} - 1) \\ -1 & \frac{1}{2}(\sqrt{8\omega + 1} + 1) \end{bmatrix}$$

with eigenvalues given by (107). Using this decomposition in (113) yields by induction

$$\bar{\mathbf{x}}^{(t)} = \mathbf{U}(\mathbf{I} + \eta_k \beta \mathbf{D})^{t-t_k} \mathbf{U}^{-1} \mathbf{x}^{(t_k)} + \mathbf{U} [(\mathbf{I} + \eta_k \beta \mathbf{D})^{t-t_k} - \mathbf{I}] \mathbf{D}^{-1} \mathbf{U}^{-1} \mathbf{z}. \quad (114)$$

Therefore,

$$\begin{aligned} e_2^{(t)} &= \mathbf{e}_1^\top \mathbf{x}^{(t)} \leq \mathbf{e}_1^\top \bar{\mathbf{x}}^{(t)} \\ &= [m_1 \Pi_{+,t} + m_2 \Pi_{-,t}] e_3^{(t_k)} \\ &\quad + [m_3 \Pi_{+,t} + m_4 \Pi_{-,t}] e_2^{(t_k)} \\ &\quad + [m_5 (\Pi_{+,t} - 1) + m_6 (\Pi_{-,t} - 1)] \delta / \beta, \end{aligned} \quad (115)$$

where we have defined $\Pi_{\{+,-\},t} = [1 + \eta_k \beta \lambda_{\{+,-\}}]^{t-t_k}$ and constants m_1 - m_8 as

$$m_1 \triangleq [\mathbf{U}]_{1,1} [\mathbf{U}^{-1}]_{1,2} = \frac{2\omega}{\sqrt{8\omega + 1}}, \quad (116)$$

$$m_2 \triangleq [\mathbf{U}]_{1,2} [\mathbf{U}^{-1}]_{2,2} = -m_1, \quad (117)$$

$$m_3 \triangleq [\mathbf{U}]_{1,1} [\mathbf{U}^{-1}]_{1,1} = \frac{\sqrt{8\omega + 1} + 1}{2\sqrt{8\omega + 1}}, \quad (118)$$

$$m_4 \triangleq [\mathbf{U}]_{1,2} [\mathbf{U}^{-1}]_{2,1} = 1 - m_3 \geq 0, \quad (119)$$

$$m_5 \triangleq [\mathbf{U}]_{1,1}[\mathbf{D}^{-1}\mathbf{U}^{-1}]_{1,1} = \frac{\mu(\sqrt{8\omega+1}+1)+4\omega\beta}{-2\beta\lambda_+\lambda_-\sqrt{8\omega+1}} = \frac{\sqrt{8\omega+1}+1}{2\sqrt{8\omega+1}\lambda_+} \geq 0, \quad (120)$$

$$m_6 \triangleq [\mathbf{U}]_{1,2}[\mathbf{D}^{-1}\mathbf{U}^{-1}]_{2,1} = \frac{\mu(\sqrt{8\omega+1}-1)-4\omega\beta}{-2\beta\lambda_+\lambda_-\sqrt{8\omega+1}} = \frac{\sqrt{8\omega+1}-1}{-2\sqrt{8\omega+1}\lambda_-} \leq 0. \quad (121)$$

Since $\Pi_{-,t} \leq \Pi_{+,t}$, $\Pi_{+,t} - \Pi_{-,t} \leq 2[\Pi_{+,t} - 1]$, $m_3 + m_4 = 1$ and $\Pi_{-,t} - 1 \geq -(\Pi_{+,t} - 1)$, we can further upper bound

$$e_2^{(t)} \leq \frac{4\omega}{\sqrt{8\omega+1}}[\Pi_{+,t} - 1]e_3^{(t_k)} + \Pi_{+,t}e_2^{(t_k)} + \frac{\mu}{-\beta^2\lambda_+\lambda_-}(\Pi_{+,t} - 1)\delta. \quad (122)$$

Similarly, from the expression of $\bar{\mathbf{x}}^{(t)}$ above, we find

$$\begin{aligned} e_3^{(t)} &= \mathbf{e}_2^\top \mathbf{x}^{(t)} \leq \mathbf{e}_2^\top \bar{\mathbf{x}}^{(t)} \\ &= [g_1\Pi_{+,t} + g_2\Pi_{-,t}]e_3^{(t_k)} \\ &\quad + [g_3\Pi_{+,t} + g_4\Pi_{-,t}]e_2^{(t_k)} \\ &\quad + [g_5(\Pi_{+,t} - 1) + g_6(\Pi_{-,t} - 1)]\delta/\beta, \end{aligned} \quad (123)$$

where we have defined g_1 - g_8 as

$$g_1 \triangleq [\mathbf{U}]_{2,1}[\mathbf{U}^{-1}]_{1,2} = \frac{1}{2}(1 - \frac{1}{\sqrt{8\omega+1}}) \geq 0, \quad (124)$$

$$g_2 \triangleq [\mathbf{U}]_{2,2}[\mathbf{U}^{-1}]_{2,2} = \frac{1}{2}(1 + \frac{1}{\sqrt{8\omega+1}}) = 1 - g_1 \geq 0, \quad (125)$$

$$g_3 \triangleq [\mathbf{U}]_{2,1}[\mathbf{U}^{-1}]_{1,1} = \frac{1}{\sqrt{8\omega+1}} \in [1/3, 1], \quad (126)$$

$$g_4 \triangleq [\mathbf{U}]_{2,2}[\mathbf{U}^{-1}]_{2,1} = -g_3, \quad (127)$$

$$g_5 \triangleq [\mathbf{U}]_{2,1}[\mathbf{D}^{-1}\mathbf{U}^{-1}]_{1,1} = \frac{1}{\lambda_+\sqrt{1+8\omega}} \geq 0, \quad (128)$$

$$g_6 \triangleq [\mathbf{U}]_{2,2}[\mathbf{D}^{-1}\mathbf{U}^{-1}]_{2,1} = \frac{1}{-\lambda_-\sqrt{1+8\omega}} \geq 0. \quad (129)$$

Since $\Pi_{+,t} - \Pi_{-,t} \leq 2[\Pi_{+,t} - 1]$ and $g_4 = -g_3$, we can further upper bound e_3 as

$$\begin{aligned} e_3^{(t)} &\leq [g_1\Pi_{+,t} + g_2\Pi_{-,t}]e_3^{(t_k)} \\ &\quad + 2g_3[\Pi_{+,t} - 1]e_2^{(t_k)} \\ &\quad + [g_5(\Pi_{+,t} - 1) + g_6(\Pi_{-,t} - 1)]\delta/\beta. \end{aligned} \quad (130)$$

Next, we use these results to bound e_2 and e_3 at global synchronization.

C. Obtaining the upper bound of $e_2^{(t_{k+1})}$ at global synchronization.

To obtain the behavior of $\bar{\mathbf{v}}_c^{(t_{k+1})} - \bar{\mathbf{v}}^{(t_{k+1})}$ after global synchronization, we use the definition of $\bar{\mathbf{v}}_c^{(t)}$, $\bar{\mathbf{v}}^{(t)}$ and the global synchronization scheme in (16), we have

$$\begin{aligned}\bar{\mathbf{v}}_c^{(t_{k+1})} - \bar{\mathbf{v}}^{(t_{k+1})} &= (1 - \alpha)(\bar{\mathbf{v}}_c^{(t_{k+1}-\Delta)} - \bar{\mathbf{v}}^{(t_{k+1}-\Delta)}) + \alpha(\tilde{\mathbf{v}}_c^{(t_{k+1})} - \tilde{\mathbf{v}}^{(t_{k+1})}) \\ &= \alpha(\tilde{\mathbf{v}}_c^{(t_{k+1})} - \tilde{\mathbf{v}}^{(t_{k+1})}),\end{aligned}\quad (131)$$

where $\tilde{\mathbf{v}}^{(t_{k+1})}$ is the global noise-free variable right before global synchronization, as opposed to $\mathbf{v}^{(t_{k+1})}$ defined right after global synchronization. Taking the norm of both hand sides of the above equality and adding over $\sum_c \rho_c$ yields

$$e_2^{(t_{k+1})} = \sum_c \rho_c \|\bar{\mathbf{v}}_c^{(t_{k+1})} - \bar{\mathbf{v}}^{(t_{k+1})}\| = \alpha \sum_c \rho_c \|\tilde{\mathbf{v}}_c^{(t_{k+1})} - \tilde{\mathbf{v}}^{(t_{k+1})}\|. \quad (132)$$

Note that, since $\tilde{\mathbf{v}}_c^{(t_{k+1})}$ represents the noise-free variable right before the global synchronization, the right hand side above can be bounded via (122), yielding the final result (104).

D. Obtaining upper bound of $e_3^{(t_{k+1})}$ at global synchronization.

To obtain the behavior of $\bar{\mathbf{v}}^{(t_{k+1})} - \mathbf{w}^*$ after global synchronization, we use the definition of $\bar{\mathbf{v}}^{(t)}$ and the global synchronization scheme in (16), we have

$$\bar{\mathbf{v}}^{(t_{k+1})} - \mathbf{w}^* = (1 - \alpha)[\bar{\mathbf{v}}^{(t_{k+1}-\Delta)} - \mathbf{w}^*] + \alpha[\tilde{\mathbf{v}}^{(t_{k+1})} - \mathbf{w}^*]. \quad (133)$$

Note that $\tilde{\mathbf{v}}^{(t)}$ is equivalent to $\bar{\mathbf{v}}^{(t)}$ before conducting global synchronization. Taking the norm of both hand sides of the above equality and applying the triangle inequality gives us

$$e_3^{(t_{k+1})} = \|\bar{\mathbf{v}}^{(t_{k+1})} - \mathbf{w}^*\| \leq (1 - \alpha)\|\bar{\mathbf{v}}^{(t_{k+1}-\Delta)} - \mathbf{w}^*\| + \alpha\|\tilde{\mathbf{v}}^{(t_{k+1})} - \mathbf{w}^*\|. \quad (134)$$

We further upper bound the right hand using (130) to obtain the result in(105). \square

Fact 1. Consider n random real-valued vectors $\mathbf{x}_1, \dots, \mathbf{x}_n \in \mathbb{R}^m$, the following inequality holds:

$$\sqrt{\mathbb{E} \left[\left\| \sum_{i=1}^n \mathbf{x}_i \right\|^2 \right]} \leq \sum_{i=1}^n \sqrt{\mathbb{E}[\|\mathbf{x}_i\|^2]}. \quad (135)$$

Proof. Note that

$$\sqrt{\mathbb{E} \left[\left\| \sum_{i=1}^n \mathbf{x}_i \right\|^2 \right]} = \sqrt{\sum_{i,j=1}^n \mathbb{E}[\mathbf{x}_i^\top \mathbf{x}_j]} \stackrel{(a)}{\leq} \sum_{i,j=1}^n \sqrt{\mathbb{E}[\|\mathbf{x}_i\|^2] \mathbb{E}[\|\mathbf{x}_j\|^2]} = \sum_{i=1}^n \sqrt{\mathbb{E}[\|\mathbf{x}_i\|^2]}, \quad (136)$$

where (a) follows from Holder's inequality, $\mathbb{E}[|XY|] \leq \sqrt{\mathbb{E}[|X|^2]\mathbb{E}[|Y|^2]}$. \square

Fact 2. Let $f(\cdot)$ be μ -strong convex and β -smooth and $\eta \leq \frac{2}{\beta+\mu}$, the following inequality holds

$$\|\mathbf{w}_1 - \mathbf{w}_2 - \eta(\nabla f(\mathbf{w}_1) - \nabla f(\mathbf{w}_2))\| \leq (1 - \mu\eta) \|\mathbf{w}_1 - \mathbf{w}_2\|, \quad \forall \mathbf{w}_1, \mathbf{w}_2 \in \mathbb{R}^M. \quad (137)$$

Proof.

$$\begin{aligned} & \|\mathbf{w}_1 - \mathbf{w}_2 - \eta(\nabla f(\mathbf{w}_1) - \nabla f(\mathbf{w}_2))\| \\ &= \sqrt{\|\mathbf{w}_1 - \mathbf{w}_2\|^2 + \eta^2 \|\nabla f(\mathbf{w}_1) - \nabla f(\mathbf{w}_2)\|^2 - 2\eta(\mathbf{w}_1 - \mathbf{w}_2)^\top (\nabla f(\mathbf{w}_1) - \nabla f(\mathbf{w}_2))} \\ &\stackrel{(a)}{\leq} \sqrt{\left(1 - \eta \frac{2\mu\beta}{\mu + \beta}\right) \|\mathbf{w}_1 - \mathbf{w}_2\|^2 - \eta \left(\frac{2}{\mu + \beta} - \eta\right) \|\nabla f(\mathbf{w}_1) - \nabla f(\mathbf{w}_2)\|^2} \\ &\stackrel{(b)}{\leq} (1 - \eta\mu) \|\mathbf{w}_1 - \mathbf{w}_2\|, \end{aligned} \quad (138)$$

where (a) comes from [43, Theorem 2.1.12], i.e., $(\mathbf{w}_1 - \mathbf{w}_2)^\top (\nabla f(\mathbf{w}_1) - \nabla f(\mathbf{w}_2)) \geq \frac{\mu\beta}{\mu+\beta} \|\mathbf{w}_1 - \mathbf{w}_2\|^2 + \frac{1}{\mu+\beta} \|\nabla f(\mathbf{w}_1) - \nabla f(\mathbf{w}_2)\|^2$ and (b) results from $\|\nabla f(\mathbf{w}_1) - \nabla f(\mathbf{w}_2)\| \geq \mu \|\mathbf{w}_1 - \mathbf{w}_2\|$ (strong convexity) and $\eta \leq \frac{2}{\mu+\beta}$. \square